DETECTION OF DELAMINATIONS OF FRP RETROFITTED REINFORCED CONCRETE COLUMNS

By

ALAN BENJAMIN KUPER

A thesis submitted in partial fulfillment of
the requirements for the degree of

MASTER OF SCIENCE IN CIVIL ENGINEERING

WASHINGTON STATE UNIVERSITY
Department of Civil and Environmental Engineering

DECEMBER 2009

To the Faculty of Washington State University:

The members of the Committee appointed to examine the thesis of ALAN BENJAMIN KUPER find it satisfactory and recommend that it be accepted.

_____
Mohamed ElGawayd, Ph.D., Chair

_____
David Pollock, Ph.D.

_____
William Cofer, Ph.D.

AKNOWLEDGEMENT

Thank you mom, dad, and Jessica for you help and encouragement. Without it I would not be where I am today.

Also, I would like to thank Maf for being tolerant with me and keeping me on track when I strayed from the path.

Karl, without your help and coaching I am sure I would still be in the lab.

Finally, this project would not have been possible with out the proposal from Dr. ElGawady and the funding provided by the U.S. Department of Transportation (USDOT), Transportation Northwest (TransNow) Regional Research Center.

DETECTION OF DELAMINATIONS OF FRP RETROFITTED

REINFORCED CONCRETE COLUMNS

Abstract

by Alan Benjamin Kuper, M.S.
Washington State University
December 2009

Chair: Mohamed ElGawady

The research presented investigates the use of a two probe configuration (transmit and receive) to detect the delamination of fiber reinforcing polymer (FRP) from reinforced concrete (RC). Current methods of detection involve visual inspection and soundings via tapping on the surface with a hammer. These methods are very time consuming, require the presence of an inspector, and possibly additional equipment such as a man lift or ladder. The method under investigation utilizes piezoelectric transducers (PZT), which have the potential to continuously test for delamination and electronically notify when the presence of an inspector is necessary.

It was found that commercial probes coupled at an incident angle of 30 degrees and transmitting in the range of 30 kHz to 100 kHz and with a separation of 720 mm were

able to detect a 20 mm delamination located between the probes. This method was also found effective on delaminations of FRP wrapped slabs, FRP wrapped full depth column specimens, and sub-strata delaminations in RC at the depth of the confining steel. The same tests were repeated with PZT wafers adhered to the slab specimen, in place of the coupled commercial probes. The initial results were lacking in the consistency in results that was found using the commercial probes and would require further research.

Table of Contents

Table of Figures

Table of Tables

Chapter 1: Introduction

1.1 Overview

Due to aging, environmental conditions, and improvement in seismic codes, the need to strengthen reinforced concrete (RC) bridges has become necessary. Because of their extremely low weight to strength ratio, immunity to corrosion, and their ease of application, fiber reinforced polymers (FRP) have gained popularity in strengthening of infrastructures.

The degradation of strength and stiffness of FRP overlays on concrete substrate may result from: a) degradation of the composite overlay; b) deterioration of the concrete substrate; or c) loss of adhesion between the overlay and the substrate. Out of these reasons, the durability of the bond between the composite and the substrate remains a critical issue. A sudden loss of the bond between concrete and the FRP can lead to a catastrophic failure of the structure (Giurgiutiu et al. 2003). Hence, early detection of FRP debonding is of paramount importance for preventing failure of strengthened structure members. Currently, Departments of Transportation (DOTs) use tap tests to detect debond in FRP. However, the tap test cannot establish the full characteristics and details of defects and it cannot be implemented in a real-time structural health monitoring (SHM). A tap test is time consuming, difficult to conduct in structural components that are difficult to access, not effective for all applications of FRP, limited to defects larger than 1 inch diameter, affected by environmental noise, and affected by the hearing ability of inspector. Finally, its accuracy rating is only medium (NCHRP 2006, Hong and Harichandran 2005).

Structural health monitoring (SHM) can be used for early detection of FRP debonding and if adequate measurements are applied, brittle failure can be prevented. SHM can be carried out using piezoelectric (PZT) sensors that are mounted on a structure. The PZT sensors send mechanical waves which are received by another PZT sensor. By examining the received signal, deficiencies in the structural element can be detected. This research investigates the use of guided waves that are created using commercial PZT or probes to detect delaminations in reinforced concrete columns retrofitted using FRP.

1.2 Objectives

The main objective of this research is to investigate the success of using Lamb waves for detecting and assessing delaminations of FRP in a retrofitted reinforced concrete element. Two types of delaminations were investigated, namely FRP delamination and cover delaminations. FRP delamination is a loss of adhesion between the overlay and the substrate, i.e. a failure in the plane along the FRP/concrete interface. Cover debonding is a loss of the substrate, i.e. a failure of the concrete in the plane of the steel rebar. The specific objectives included:

- Determine the best practice test set-up and required equipment to effectively inspect delaminated regions of retrofitted elements,
- Determine if Lamb waves are able to detect and assess the existence of FRP and/or concrete cover delaminations.
- Determine if Lamb waves will be able to determine the near field and far field delaminations.
- Determine the thickness of FRP for which Lamb waves can be used to detect FRP delaminations.

To achieve these objectives three slabs of approximately 50 mm x 400 mm x 900 mm representing a concrete substrate and one column 400 mm x 400 mm x 900 mm were constructed and tested. Different surfaces and locations of the specimens had different conditions. These included concrete surfaces that do not have any anomaly, well FRP-retrofitted surface, FRP delaminated surface, and debond of the concrete substrate. In addition the delaminated surfaces had different delamination sizes and different amounts of FRP.

1.3 Report organization

This thesis consists of 5 chapters. First, it starts with a description of the problem statement, and objectives. Chapter 2 discusses work carried out by other researchers in the area of Lamb waves and structural health monitoring. Chapter 3 describes experimental work. Chapter 4 discusses the experimental results. Finally, chapter 5 is a conclusion of this thesis.

Chapter 2: Literature Review and Background

2.1 Guided Waves

One emerging candidate for FRP delamination detection is the use of guided waves (Lamb waves) as it is a reliable and cost effective technique. Rose (1999) estimated that the cost of structural health monitoring (SHM) using Lamb waves is about 1/20 of other standard inspection techniques. Waves are mechanical disturbances that travel in a medium with finite velocities. If the medium is unbounded, two kinds of waves with different velocities- shear (S) and longitudinal (P) waves- can propagate independently. These waves together are called bulk waves. The existence of a boundary or interface between two different solids will introduce coupling between P- and S-waves, i.e. a reflected S-wave can be generated from an incident P-wave, and conversely, a reflected P-wave can be generated from an incident S-wave. Now if there are two parallel boundaries such as an infinite plate, those reflected P- and S-waves will be reflected back and forth between the two boundaries, and a large number of new P- and S-waves will be generated. The interferences of all P and S-waves become a new kind of wave propagating in the direction of the two boundaries. These waves are called guided waves because they propagate as if they are guided by the two boundaries (Luangvilai 2007). The plate conditions are met when the wavelength (λ) is approximately 3 to 10 times the plate thickness (Bray and Stanley 1997, Huang 1999).

The remaining dimensions of the plate must be much greater than the wavelength to be considered as an infinite plate.

There are an infinite number of Lamb wave modes that can propagate in a plate. These modes can be classified into two main groups dependent on the particle

displacement (symmetrical and anti-symmetrical) form (Jung et al. 2001). The velocity of each mode varies with the frequency. This nature is called dispersion.

Plate, or Lamb, waves are commonly used to test plates for anomalies such as steel delaminations, corrosion, concrete honeycomb, or change in material properties. These waves are ideal for analyzing plates because they are easily definable given the material constants of the longitudinal and shear wave speed, which are definable from the density, Poisson's ratio, and Young's modulus. With these properties all the modes of dispersion can be defined.

2.2 Delamination detection

Kundu (2002) was successful in detecting delamination of steel rebar from concrete in RC structures. By coupling a probe to the end of an exposed rebar, it could determine the length of the delamination. The frequency that produced the greatest amplitude was selected to measure flaw detection. It was found that as the delamination increased, the amplitude of the reflected wave increased. This was due to the energy reflecting off the free surface and back into the steel instead of passing through into the concrete, causing it to attenuate rapidly.

The comparison of the frequency's amplitude to detect FRP delamination was also utilized by Giurgiutiu et al (2003). Piezoelectric (PZT) wafers were applied to the surface of FRP layers and then the layers were debonded from the surface of a reinforced concrete beam while the impedance was recorded. This method found that as the size of the delamination region increased, the impedance amplitude increased. The position of delamination was detectable using a damage index, which was found through a

Euclidiean based equation comparing the impedance amplitude of the healthy and delaminated beam.

In work done by Tucker (2001), Lamb waves were used to detect delamiation within wood veneer. It was found that delamination led to a decrease in the frequency thickness value of the dispersion curve. A similar method was used by Luangvilai (2002) to study delaminations. By using a computer program to analyze the data, human interpretation was removed and large sets of data could be rapidly analyzed. This method was able to analyze a signal with many overlapping modes and frequencies.

Chapter 3: Experimental Work

3.1 Test Specimens

Three substrate specimens of approximately 50 mm x 400 mm x 900 mm representing a concrete substrate and one column of 400 mm x 400 mm x 900 mm were constructed during the course of this experimental work. The first substrate specimen, Sub-C, represents the concrete cover of an un-retrofitted concrete column free of any anomalies. To use material efficiently, the second substrate specimen was built to represent two different damage states. The first part of the specimen was well retrofitted, i.e. with no delaminations (Figure 1). From here on, Sub-R1 will refer to the part of the specimen that was well retrofitted. The second half of the slab had a delamination of variable size ranging from zero to 230 mm in length. Sub-D1 refers to the delaminated part of this specimen. The last substrate specimen was similar to the second substrate (Figure 1) but with three FRP layers. Sub-R3 refers to the well retrofitted part of this specimen and Sub-D3 refers to the delaminated part of this specimen.

For the column specimen, three sides of the column were used to investigate three different damage states. One surface contained no FRP i.e. just a concrete surface, this surface hereinafter referred to as specimen Col-C. The second surface contained a substrata debonding i.e. separation between the stirrups and the approximate 52 mm cover of concrete, this surface hereinafter referred to as specimen Col-B. The third surface contained a delmaination similar to that of Sub-D1 i.e. with variable size (Figure 2 and Figure 3), this surface hereinafter referred to as specimen Col-D1. The substrata debonding is at maximum 254 mm wide for a length of 60 mm; then, tapers to a point over the length of approximately 340 mm.

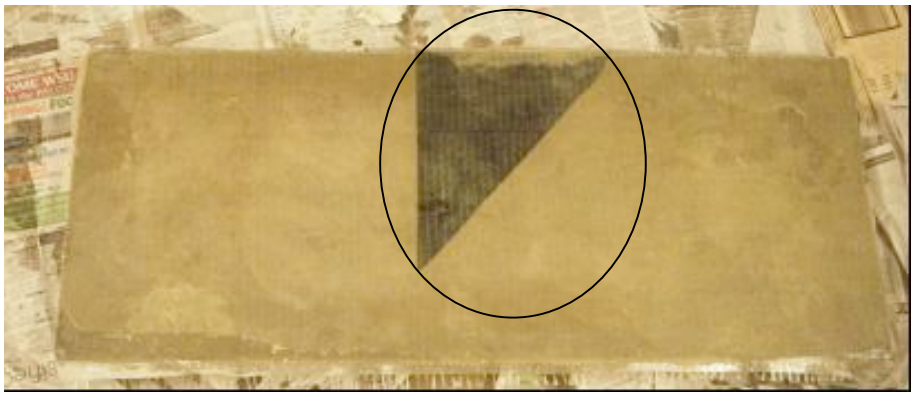

Figure 1. Retrofitted slab specimen with varying length delamination

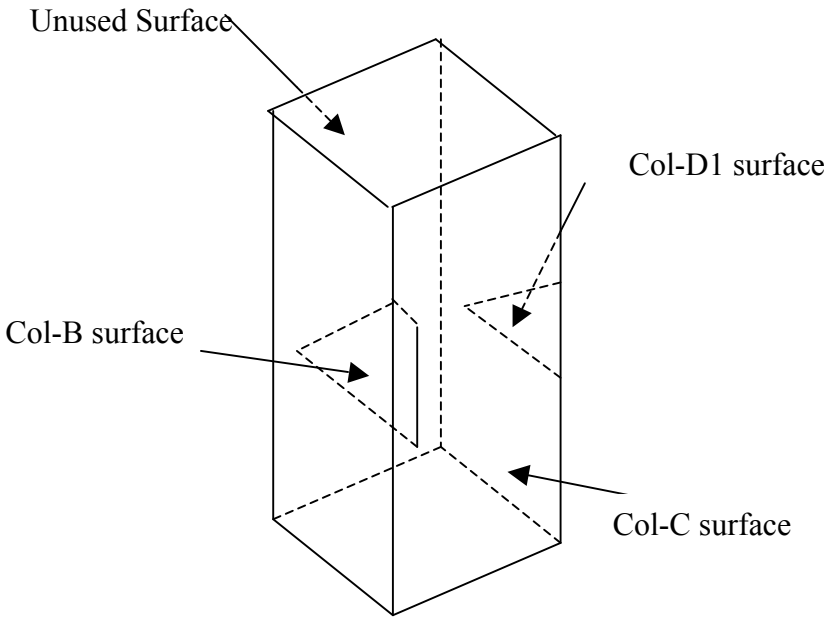

Figure 2. Column Specimen

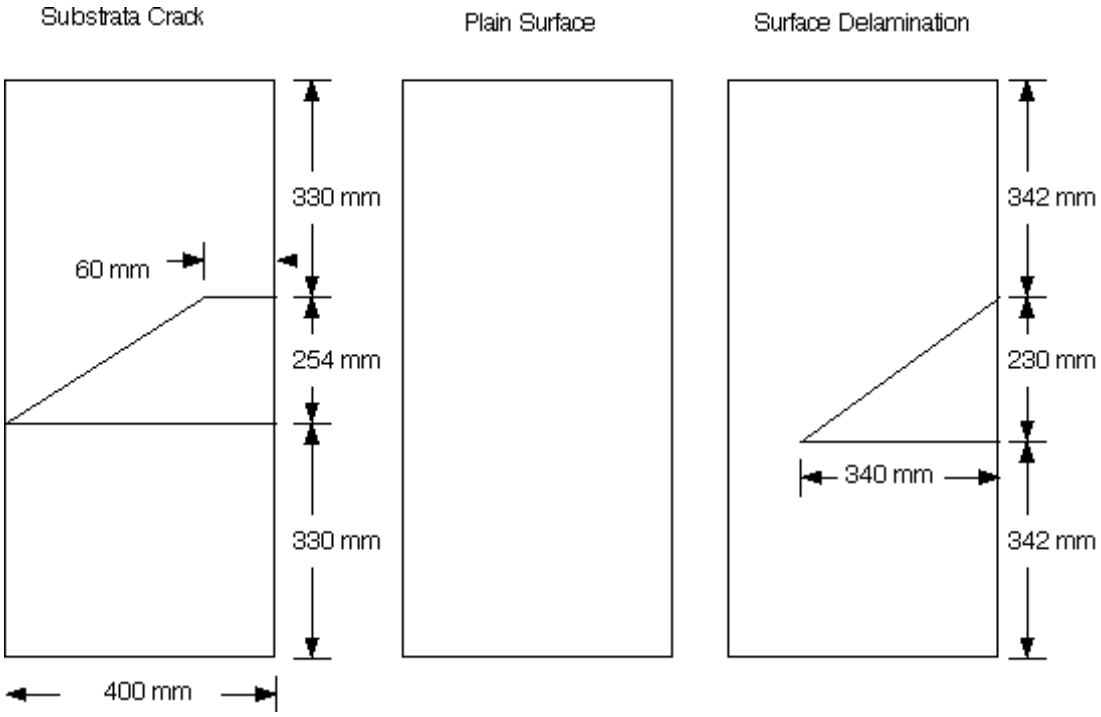

Figure 3. Dimensions of Column

The slabs were used to investigate whether or not Lamb waves are able to detect the presence and size of delamination. Also, it was used to investigate the effect of distance between the transducer/receiver and the delaminated area as well as the number of layers of FRP on the propagation of Lamb waves. The column was used to detect a substrata crack which is typical of an over stressed RC member. Also, it was used to determine the effects of increasing the depth of the concrete element on propagation and detection of the Lamb waves.

The test samples were created using Melamine coated particle board. The concrete used was a premix with the strength of 39 MPa. Using melamine for form work provides a very smooth surface because the cement does not adhere to the plastic coating. The smooth surface was ideal for coupling the wedge to the concrete. By keeping the surfaces smooth, the surface can better represent a plate. This is not typical in actual concrete columns but will increase the likelihood of lamb wave propagation. For the

retrofitted specimens, the specimens were coated on the specified surface with QuakeBond™ J300SR epoxy. Next, the FRP was carefully placed onto the surface and fully impregnated with epoxy. A waxed piece of laminate, typically used to cover countertops, was carefully placed onto the surface and weighted in place until the epoxy had cured at least one day. After peeling it off, a smooth surface that could be coupled to was present over the entire specimen. If a delamination of the FRP was necessary, a piece of waxed plastic was placed between the epoxy surface and the FRP before the impregnation process. The waxed plastic was then pulled out after 24 hours. This created the required length delamination of the FRP.

The formwork for the column was also constructed of melamine particle board. The steel cage of the column was made of 4 #3 longitudinal rebar of grade 60 and stirrups of #2 spaced at 100mm, as seen in Figure 4. Immediately after pouring the column specimen a 12 gauge thick steel plate, coated with bearing grease, covered with a plastic sheath, also coated in bearing grease was gently pushed into the form tightly against the stirrups, as seen in Figure 5. After curing for one day, the steel plate was pulled out of the plastic and the plastic was then removed from the void, which the steel plate left behind. This provided a substrata crack, representing a spalling effect.

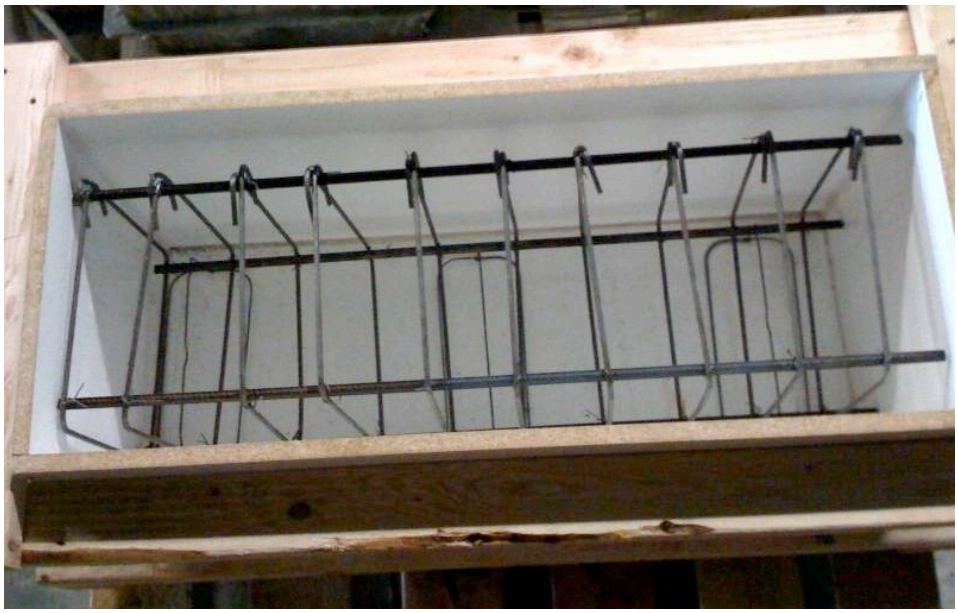

Figure 4. Column form with rebar cage

Figure 5. Column specimen with 12 gauge steel plate to create substrata crack

3.2 Test Setup

The test set-up used during this research is shown in Figure 6 and Figure 7. To synchronize the time the signal pulsed and the time the computer started recording data, the trigger of the Panametrics HV Pulser/ Receiver 5058PR was used. The frequency, amplitude, and number of sinusoidal pulses of transmitted signal were altered using a Fluke 218 Arbitrary Waveform Generator. The transmitting (T) and receiving (R) probe

used was the Panametrics Videoscan V1011. Plastic wedges were fabricated with the ability to change the transducing and receiving incident angles. Ultragel II was used as a coupling material. Before the received signal could be detected by the computer, it had to be amplified using the integrated preamp of the Pulser/ Receiver. A computer containing a National Instrument card (NI PCI-5152) and the LabVIEW program was used to view and save the received signal.

Figure 6. Standard 100 kHz probe and plastic variable angle wedge setup

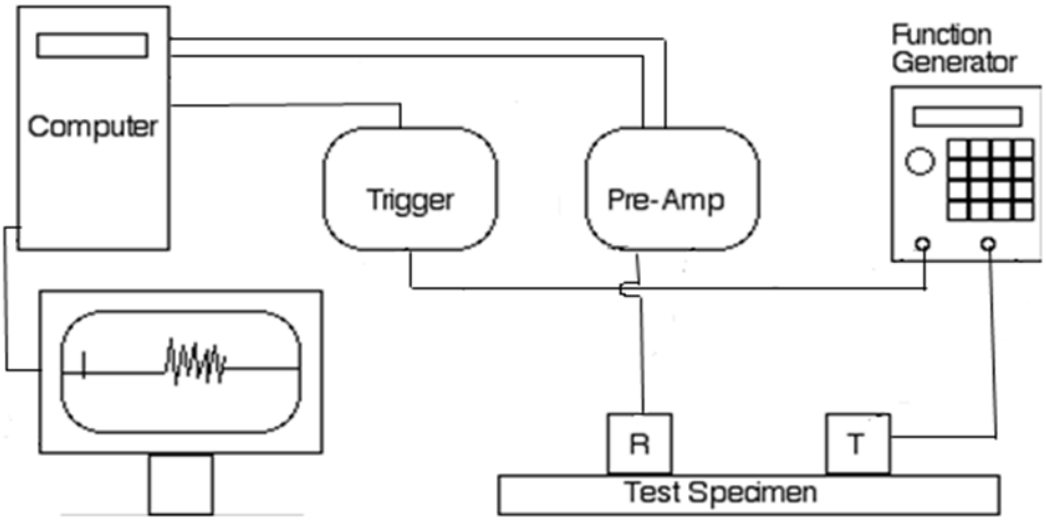

Figure 7. Test setup

It is important to note that the size of the probe had an effect on the shape of transmitted signals. The probe continued to vibrate for a short duration after the function generator stopped sending signals. Figure 8 shows the actual transmitted signal for a 100 kHz of 2 sinusoidal pulses at 1 v. It can be seen that the probe continued to vibrate for an extra 2 sine pulses of trailing vibrations. This trailing increased with increasing the voltage of the transmitted signal. With the transmitted voltage increased to 20 volts (Figure 9), the sine pulses increase and so do the trailing vibrations. Figure 9 shows that there were about an extra 2.5 sine pulses trailed by vibrations. This effect occurred for other frequencies using this probe. Note that the peak values of the 100 kHz 20 volt signal was distorted because the detectable voltage by the computer was limited to approximately 3volts.

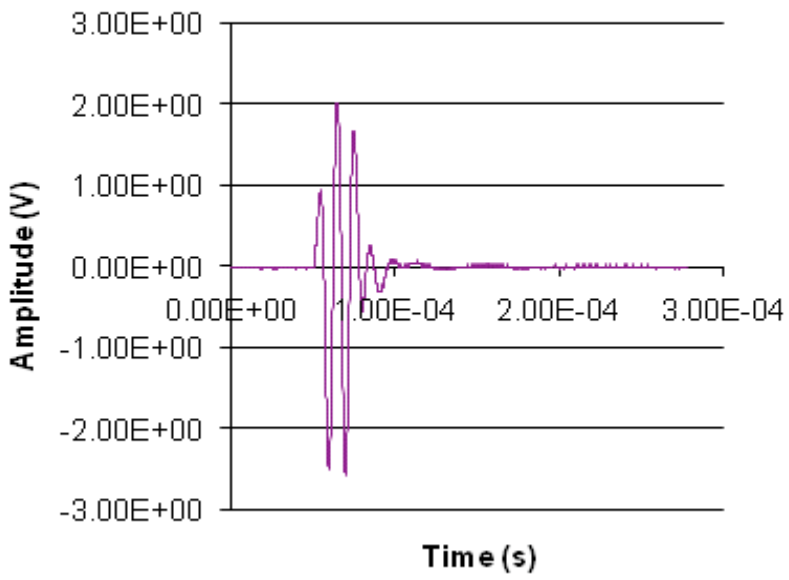

Figure 8. Actual transmitted signal of a 100kHz 2 sinusoidal pulse at 1 volt

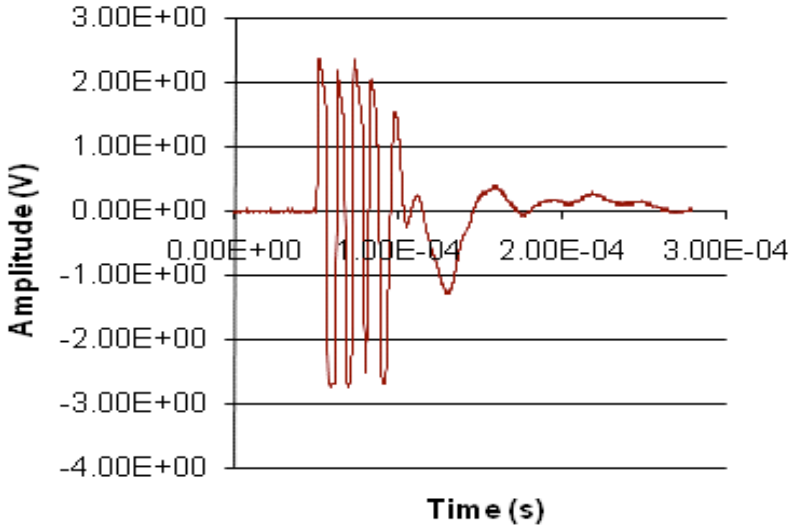

Figure 9. Trailing effect on signal consisted of 2 sinusoidal pulses at 20 volts and 100kHz

3.3 Material Properties

To define the dispersion curves for a specific material it is necessary to know two parameters, the longitudinal and shear wave speeds. For homogenous materials such as

steel or aluminum, both velocities are well reported with a very high accuracy. However, the velocity in concrete depends on the proportion of its components as well as the characteristics of its individual components such as aggregate size. Hence, the longitudinal and shear velocities need to be experimentally determined for the concrete used in this research.

The longitudinal speed was determined by placing a probe on each end of specimen Sub-C. A signal (Figure 10) was transmitted at 100 kHz over a distance of 318 mm. The time difference was taken from the initial pulse from the transmitting probe to the first detection of the pulse by the receiving probe. The longitudinal velocity of the concrete was found to be 3978.7 m/s, which will be used as c_1. Values in the order of 4056 m/s were reported in the literature (e.g. Al Wardany et al 2007). There is a possibility that the velocity was affected by the geometric properties of the specimen on which it was tested. The test was measured at 100 kHz and the specimen thickness was 50 mm, which means waveguide effects could have taken place. Therefore, the velocity measured could have been closer or somewhere between the bulk velocity (c_1) and the longitudinal wave velocity (c_l). For the following test, the value determined above will be accepted as the bulk velocity.

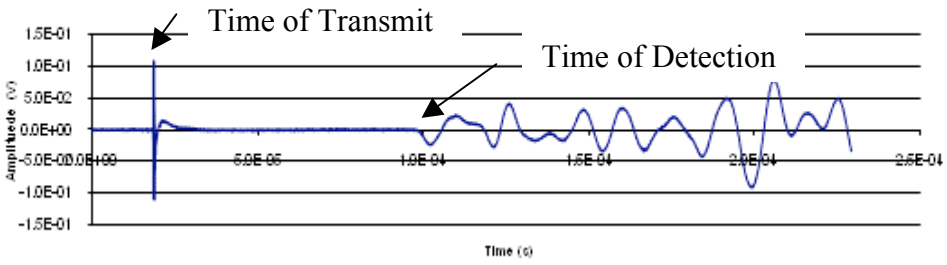

Figure 10. Longitudinal wave in concrete

The measured longitudinal wave velocity was used to calculate the shear wave velocity using Equations 1 and 2.These equations can be simplified to Equations 3 and 4, as shown in Appendix A 1.

$$c_1 = \sqrt{\frac{\lambda + 2\mu}{\rho}} \qquad [1]$$

$$c_2 = \sqrt{\frac{\mu}{\rho}} \qquad [2]$$

$$c_1 = \sqrt{\frac{E(1-\nu)}{\rho(1+\nu)(1-2\nu)}} \qquad [3]$$

$$c_2 = \sqrt{\frac{E}{2\rho(1+\nu)}} \qquad [4]$$

Where ρ is the concrete density, measured to be 2243kg/m^3, ν is the concrete Poisson's ratio postulated as 0.2 (a commonly assumed design value), and E is the concrete Young's modulus, calculated using Equation 3 and found to be approximately 31.96 GPa which closely approximates the work done by Al Wardany (2007) where the Young's modulus was determined to be approximately 33.9 GPa. After substituting for the E, ρ, and ν values into Equation 4, the shear wave velocity (c_2) was calculated to be 2436 m/s.

3.3.1 Dispersion of Lamb waves

Lamb waves exhibit velocity dispersion; that is, their group velocity of propagation depends on the frequency (or wavelength) multiplied by the plate thickness, as well as on the elastic constants E, ν, and density of the material. The derivation of the formula that describes the dispersion curves of Lamb waves is well established in the literature (see

for example Rose (1999) and Remram et al. (2006)) and will not be repeated here. Equation 5 represents the relation between the phase velocity (c), the Lamb wave frequency (ω), and plate thickness (d). The longitudinal wave velocity (c_1) and shear wave velocity (c_2) are constant and specific for each material. The equation must be solved using a numerical procedure (Rose 1999). A program was written in MatLab to numerically solve this equation. The program can be found in Appendices A 2 and A 3. The program starts by assuming a value for the wave frequency (ω), then it iterates for a value of the phase velocity that satisfies Equation 5. Then ω is incremented and the program finds the new corresponding phase velocity that satisfies the equation. There are an infinite number of solutions to this equation but only a small region will be used based on our frequency-thickness constraints to minimize the number of modes occurring at once. Figure 11 shows the dispersion curves for a concrete plate, which will be used for the concrete slab having a thickness of 52 mm.

$$\frac{\tan(\omega d)\sqrt{(c^2 - {c_2}^2)/{c_2}^2 c^2}}{\tan(\omega d)\sqrt{(c^2 - {c_1}^2)/{c_1}^2 c^2}} + 4\left(\frac{\sqrt{\left((c/c_1)^2 - 1\right)\left((c/c_2)^2 - 1\right)}}{\left(2 - (c/c_2)^2\right)^2}\right)^{\pm 1} = 0 \qquad [5]$$

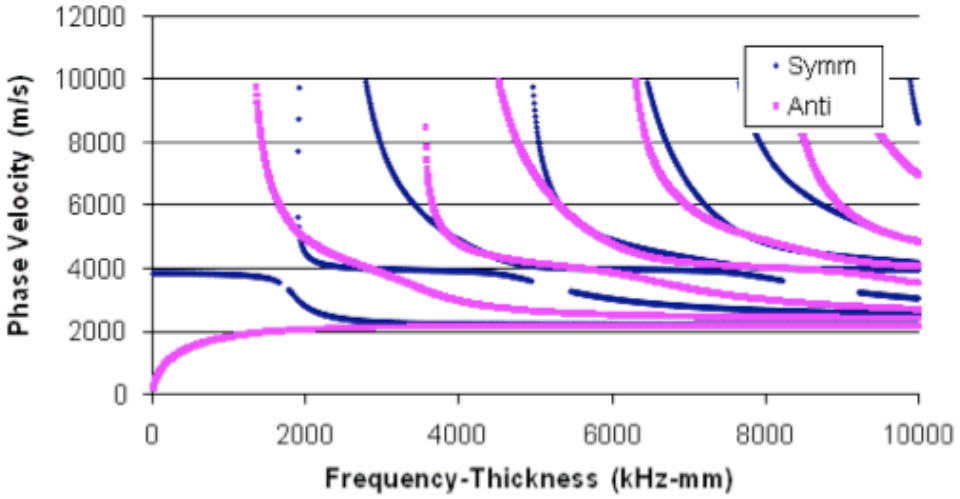

Figure 11. Dispersion curve of concrete

3.4 Test procedure

The probes were separated a known distance and a sinusoidal pulse was sent by the transmitter to the receiver. Using Snell's law, as seen in Equation 6, the appropriate angle can be used to isolate the shear or longitudinal wave. Using the function generator and variable angle wedges, the ideal angle could be selected for the specific phase velocity of the desired mode on the dispersion curve. Every test was take three times to provide variation in the signal received due to coupling inconsistencies. The longitudinal wave speed for the wedge, c_1, was taken as 2073 m/s and $\theta_2$was 90° to ensure that the signal is traveling parallel to the free surface. The variable θ_1 is the angle of the transmitting and receiving probe and could be changed freely.

$$\frac{\sin\theta_1}{c_1} = \frac{\sin\theta_2}{c_2} \qquad [6]$$

The test set-up was calibrated against tests on an Aluminum plate, first, and then carried out on the concrete specimens.

3.5 Analysis

In order to detect the flaws for the different specimens, different characteristics of the received waves were investigated. First, the dispersion curves of the different specimens were investigated to determine if there was any change in the frequency and/or velocities due to delaminations. Two methods, namely phase peaks and short-time Fourier transform (STFT), were used to experimentally determine the phase velocity as a function of wave frequency. Second, the amplitudes of the different frequencies were calculated to determine if there was any magnification in the frequency due to any sort of delaminations.

3.5.1 Phase Peaks to Determine Phase Velocity

This method was used by Tucker (2001) to determine the phase velocities of the A_0 and S_0 waves. The peaks of the received signal and their corresponding arrival times were determined. The arrival times were used to determine the phase velocity of each peak. By keeping the pulse frequency low in the range of 30 kHz or less, minimal dispersion occurs and only the lowest order of the modes should be prevalent. The velocities of the two modes were calculated and compared to those in the theoretical dispersion curve.

3.5.2 Short-time Fourier Transform (STFT) Analysis

Lamb wave signals are non-stationary, i.e. the signals' frequency contents change with time. For a signal of this type, the normal Fourier transform becomes insufficient to capture the signal's relevant characteristics because it uses the signal at all times and shows the total signal's frequency content over that period of time. Another transform called short-time Fourier transform (STFT) was developed (Luangvilai 2007) to focus on

the signal's spectrum over a short period of time. The STFT analyzes the received signal and can detect the amplitude and frequency at any particular time.

A program was written in MatLab to carry out the STFT. It can be found in Appendix IV. Initially it reads a signal that has a time domain beginning at the initial pulse. Next, it takes a small sequence (portion) at the beginning of the received signal centered at time t_i and multiplies its amplitude values by a Hanning window (Luangvilai 2007). This windowed sequence (portion) is discretely transformed by the FFT algorithm. The window is moved to another time centered at $t_i+\Delta t$ and the same procedure is repeated. By knowing the arrival time of the center of the window and its frequency, the dispersion curve can be plotted. The Matlab program extracts the maximum frequency recorded by each STFT window.

The STFT analysis method does not use differential methods to find the velocities, as does the phase peaks method, so the distance traveled in the wedges cannot be neglected. Using the longitudinal wave velocity in the wedge, the traveling time in the wedge could be calculated and subtracted from the total travel time of the wave, only accounting for the travel time in the concrete substrate. The speed of the longitudinal wave in the wedge was found using the same method used for finding the longitudinal speed of the waves in the concrete.

3.5.3 Damage Index Using Frequency Domain

The Fast Fourier Transform (FFT) analysis is a powerful mathematical procedure that can analyze a signal and decipher the frequency or frequencies, which are imbedded within the signal. The signal image was taken, encompassing the main body of the signal as well as the trailing noise until the signal neared full attenuation. With the frequency

domain for a signal, a damage index (I_D) can be generated to detect flaws. I_D is based on the Euclidian norm between the FFT for a baseline and damaged specimens. The root mean square deviation (RMSD) formula used was

$$I_D = \sqrt{\frac{\sum_{1}^{N}\left[A_i - A_i^0\right]^2}{\sum_{1}^{N}[A_i^0]^2}} \quad [7]$$

Where I_D is the damage index, A_i is the amplitude of the FFT for a given frequency (i) for a baseline specimen and A^0_i is the amplitude of the FFT for a given frequency (i) for a damaged specimen.

Chapter 4: Experimental Results

4.1 Phase Velocity Peak Value Method

4.1.1 Aluminum

This method was performed on an aluminum plate to validate the process and the test set-up. An aluminum plate approximately 4.7 mm thick was used for this validation. The separation distances between the transmitter and receiver were 149 and 258 mm. To detect the S_0 mode having approximately a velocity of 5400 m/s, 5 sinusoidal wave pulses at 90 kHz were sent at an angle of approximately 21.7° through the plate. The angles of the transmitter and receiver probes was selected using Snell's law and considering the longitudinal speed of the wave in the wedges to be approximately 2073 m/s. The result of a typical test can be seen in Figure 12 The main peaks and their arrival time were defined from this graph and the relative velocity was found by averaging the velocity of the peaks as shown in Table 1. The phase velocity of this mode was found to be approximately 5450 m/s. Given the thickness and frequency, the measured velocity could be plotted on to the dispersion curves of aluminum with a 258 mm spacing (Figure 13). The measured velocity for the S_0 mode had a strong correlation with the calculated dispersion curve. This confirmed that the experimental set-up worked well. Only the longitudinal mode was prevalent in the image so the shear mode was not considered in the test.

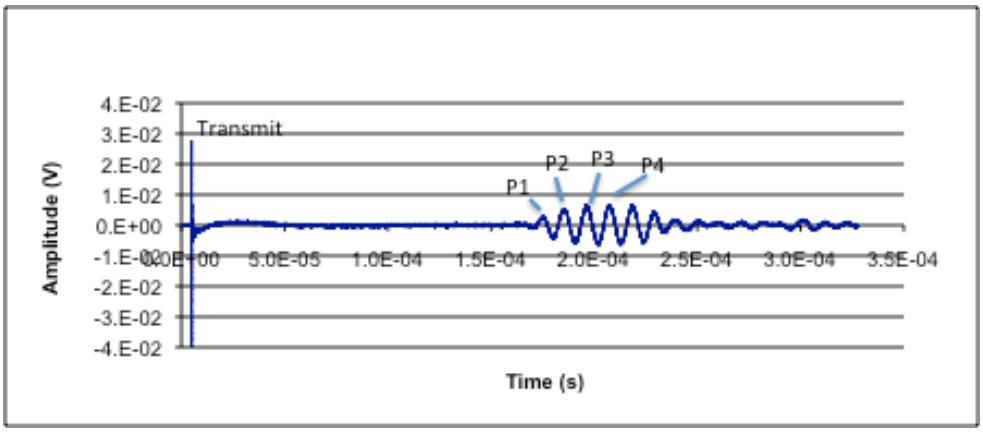

Figure 12. Received from aluminum plate at 90 kHz with incident angle of 22 degrees

Table 1. Times for each peak for aluminum phase velocity

Gap	14.9 cm	25.8 cm	Vel. (m/s)
P1 Time (s)	1.56E-04	1.77E-04	5332.7
P2 Time (s)	1.66E-04	1.86E-04	5466.4
P3 Time (s)	1.78E-04	1.98E-04	5466.4
P4 Time (s)	1.89E-04	2.09E-04	5533.0

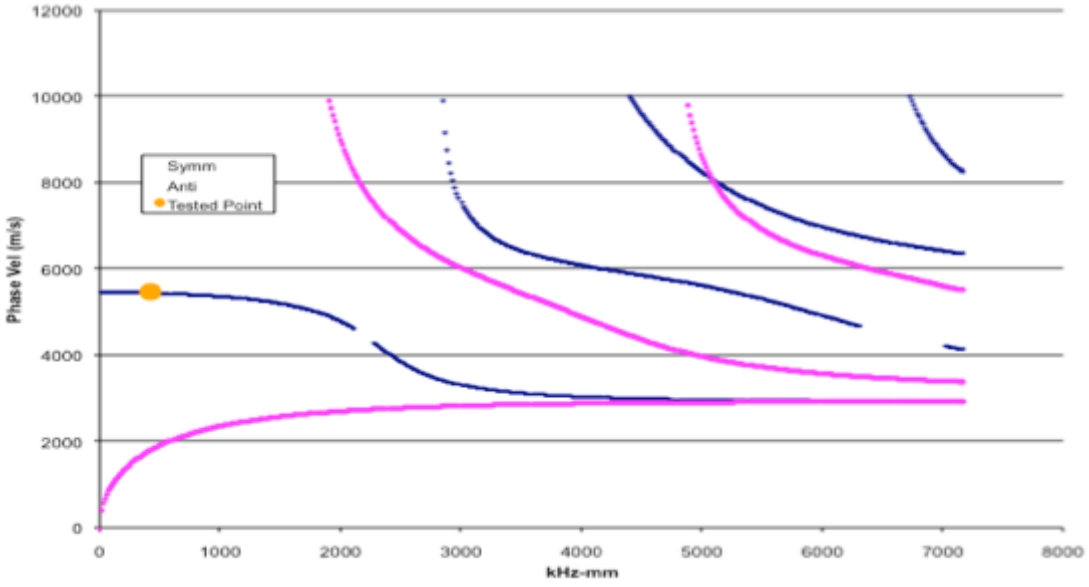

Figure 13. Aluminum dispersion curve with plotted value

4.1.2 *Concrete*

This method was applied to a concrete substrate retrofitted using FRP as shown in Figure 1. The FRP layer was approximately 1 mm thick while the concrete substrate was 52 mm thick. Hence, it was assumed that the stiffness of the fiber would be negligible compared to the concrete substrate. The concrete was tested at 36 kHz and incidence angle of 38° as well as at 40 kHz and an incidence angle of 40° to locate different points on the dispersion curve of S_o. These frequencies and velocities were chosen based on Snell's Law. Spacing of 41, 65, and 118 mm were used and the values of the arrival times of each peak of the group were recorded as shown in Table 2. A sample of the measured signal is shown in Figure 14. The recorded arrival time and the separation distance for each peak were used to calculate the average velocity as shown in Figure 15. The measured average velocity was plotted on the dispersion curves in Figure 16. As shown in the figure, using this method with retrofitted concrete substrate resulted in less accurate results compared to using the method with a homogenous material like aluminum. This could easily be due to the heterogeneity of the concrete, the composite nature of the specimen (FRP, epoxy, and concrete), and imperfections and air voids in the specimen. All of these could cause reflection and scattering of the signal.

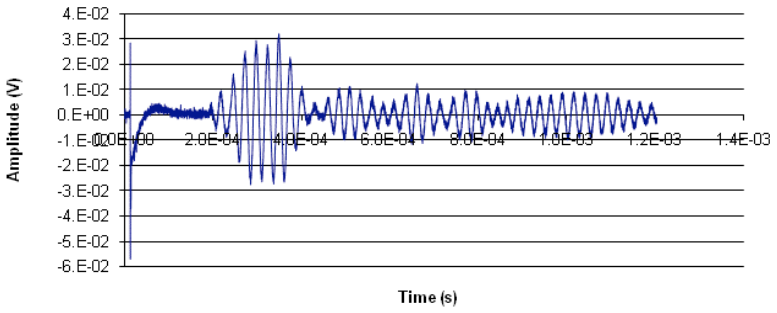

Figure 14. Specimen Sub-R1 tested at 40 kHz and incident angle of 40° with a separation between wedges of 118 mm

Table 2. Time of travel and velocity of each peak for 40kHz test

Gap	41 mm	65 mm	118 mm	Vel. (m/s)
P1 Time (s)	1.79E-04	1.87E-04	1.98E-04	4032.6
P2 Time (s)	2.02E-04	2.10E-04	2.20E-04	4265.5
P3 Time (s)	2.25E-04	2.31E-04	2.47E-04	3487.7
P4 Time (s)	2.50E-04	2.57E-04	2.73E-04	3363.9
P5 Time (s)	2.75E-04	2.83E-04	2.98E-04	3248.8

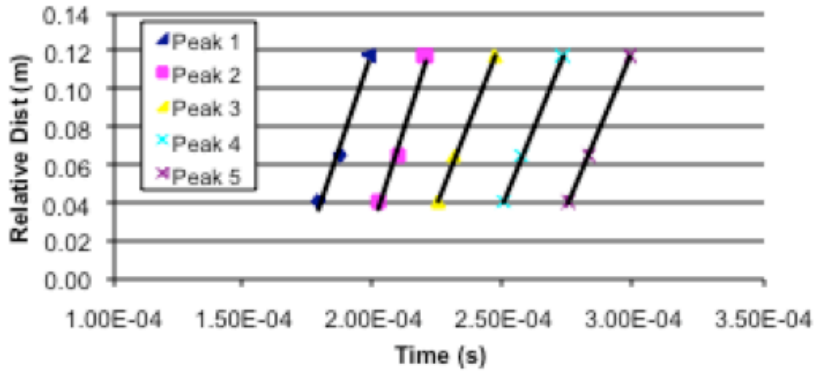

Figure 15. Calculation of the phase velocities for 40 kHz

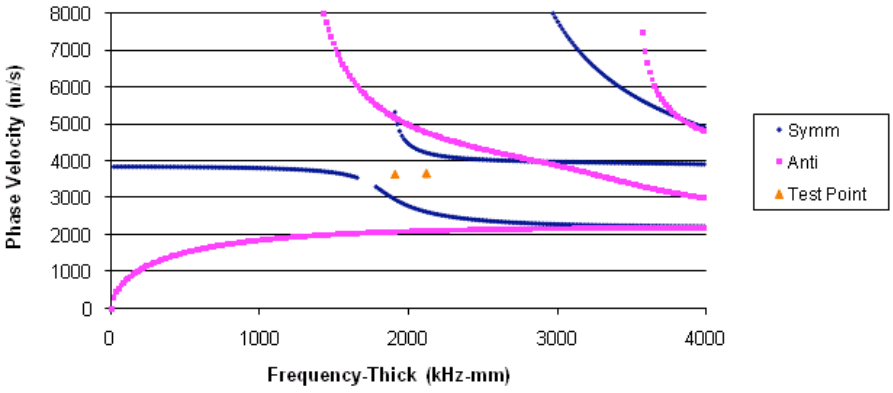

Figure 16. Retrofitted concrete dispersion curve with 36 kHz and 40 kHz tests

4.2 STFT Results

The results of the STFT depend on several factors including the window size, the sampling rate, and the number of sinusoidal pulses transmitted.

4.2.1 Window Size Variations

One of the main parameters that influence the precision of the STFT is the window size. Using a larger window size means finer-grained frequency analysis. Using a small window size results in a low frequency analysis. For a given window length, the base frequency and number of frequency components that can be analyzed are the sampling rate/window length and half the window length, respectively. Figure 17 shows the effect of the window size on detecting the different modes of the Lamb waves for the specimen Sub-R1. The test was carried out using a frequency of 40 kHz, an incident angle of 50°, and a sampling rate of approximately 6,000,000 points/sec. As shown in the figure, the window size of 100 and 200 points provided a good correlation with the theoretical dispersion curves. The 600 and 400 point windows detected the S_0 mode, but they do not detect as many orders in the 6000 kHz-mm range as did the 200 point window (Figure 17). The window size of 200 points was selected to conduct the following tests.

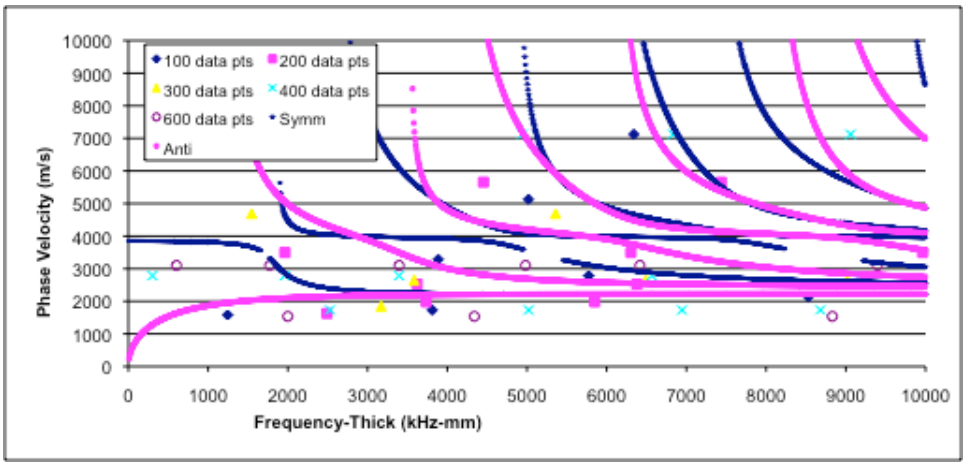

Figure 17. Variation of window size for Sub-R1 tested at 40 kHz and 50 degrees

4.2.2 Effect of Number of Sinusoidal Pulses

Five different sinusoidal pulses were tested on specimen Sub-R1. These tests used 1, 2, 5, 7, and 10 sinusoidal pulses to investigate which signal provided the best results (Figure 18 and Figure 19). It was found that 2 sinusoidal pulses produced the most correlation between the dispersion curve and test data. This was based on the data provided from the test results for the S_0 and A_0 modes, but only the 2 sine pulses provided precision with the higher modes. There are very close matches within the first, second, third, and fifth modes for the 2 sine pulse test.

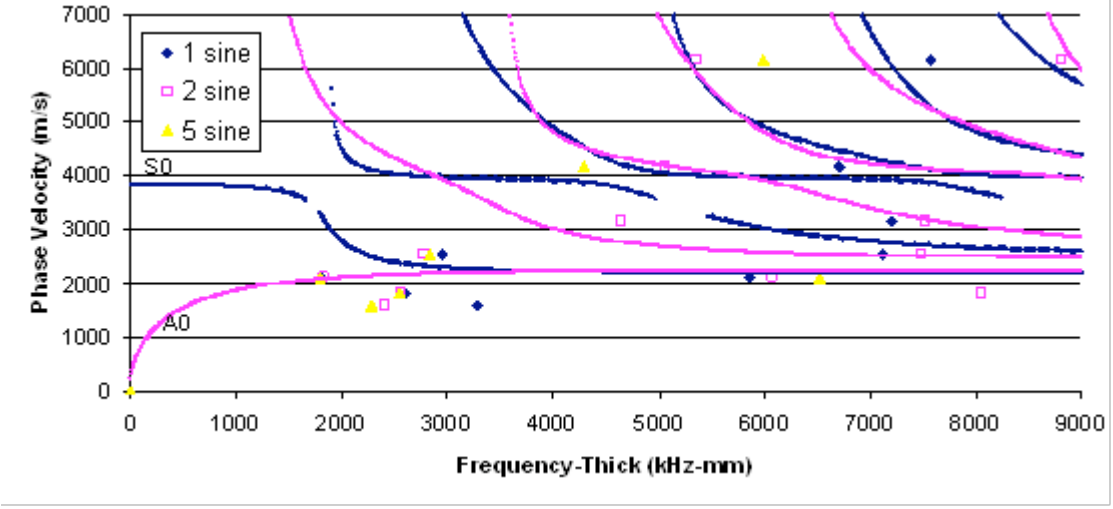

Figure 18. 1, 2 and 5 sine pulses tested at 40kHz and an incident angle of 45° over a distance of 160 mm.

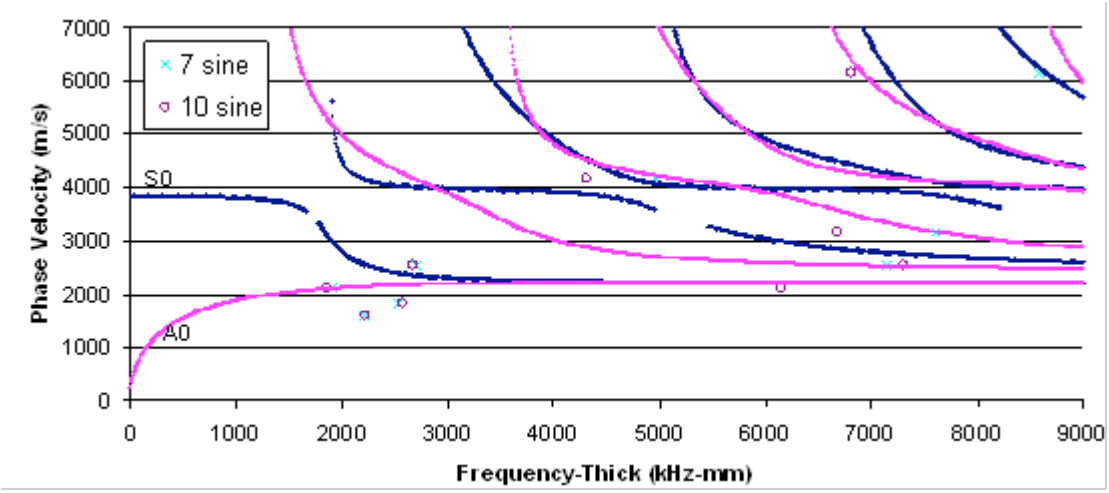

Figure 19. 7 and 10 sine pulses tested at 40kHz and angle of 45° over a distance of 16 cm

4.2.3 Effect of Incident Angle and Frequency

In this section the effects of the incident angle and frequency on the propagation of the Lamb wave modes were investigated. The investigated test angles were 20°, 30°, 40°, 45°, and 50°. These were selected on the basis of the longitudinal and shear wave speed velocities. From Snell's Law, it was found that approximately 30° was necessary to transmit the longitudinal wave across the surface. To insure that this was not beyond the critical angle for the longitudinal wave, 20 ° was also used. Likewise, the shear critical

angle was 58° which is ideal to send the shear wave parallel to the surface of the plate. The frequencies tested were 25, 30, 40, 50, and 100 kHz. The lower frequency of 25 kHz was selected since it was the lowest frequency that the probe can transmit through specimen Sub-R1 without high frequency noise. Figure 20 shows the effects of the incident angle on the detected frequencies and velocities.

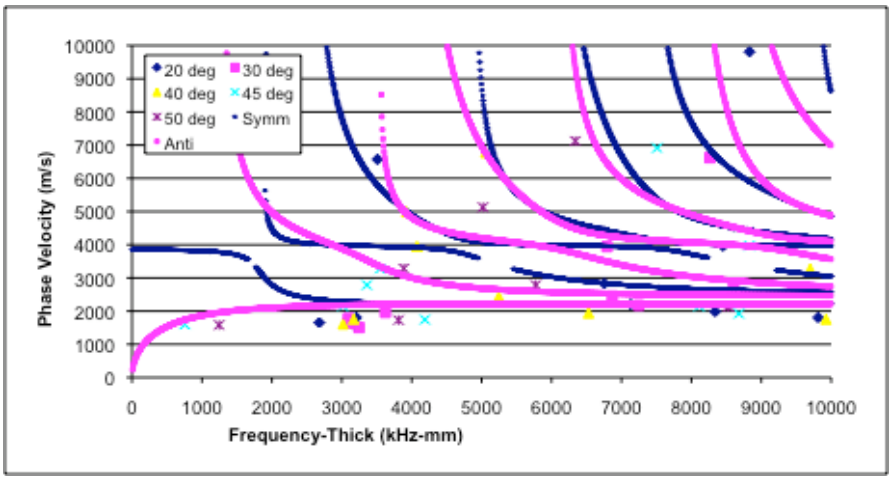

Figure 20. STFT for 40 kHz and different wedge angles

4.2.4 Delaminated specimens

In order to detect FRP delamination, the characteristics of the received signals were examined. Specimen Sub-D1 was investigated using 40 kHz and different incident angles, namely, 20°, 30°, 40°, 45°, and 50°. STFT analysis was carried out on the received signal (Figure 21). By comparing Figure 20 and Figure 21, any shift in the frequency content of the received signal due to delamination should be detected. As shown in the figures, there were some differences, but it was not possible to find a correlation between the existence of delamination and the shift on the frequency content. The results of the STFT for the different substrate specimens are presented in Appendixes B 1 and B 2.

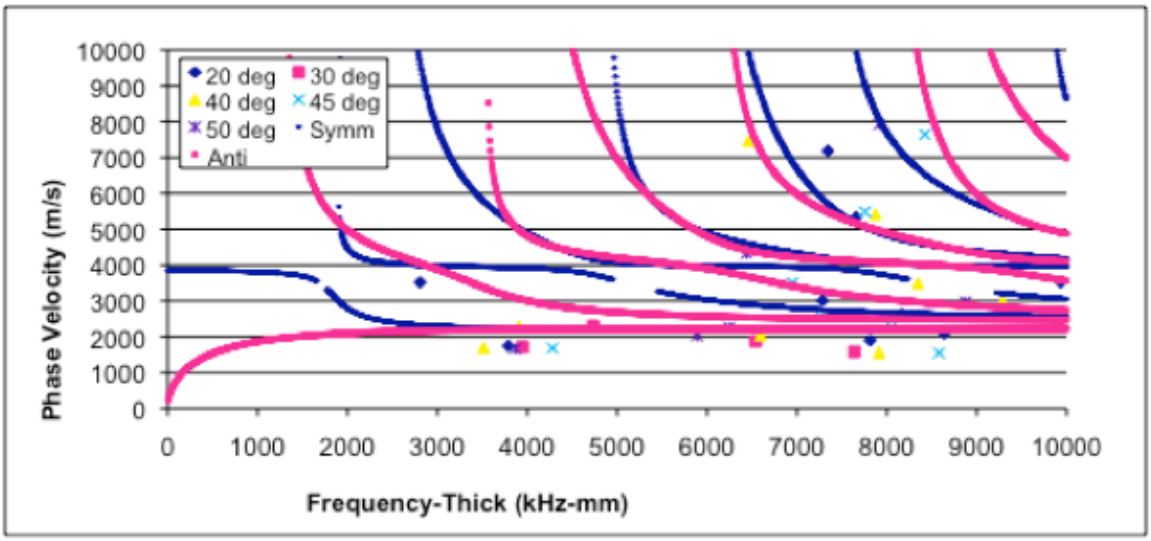

Figure 21. STFT for 40 kHz and different wedge angles for specimen Sub-D1 (having 30 mm delamination)

4.3 Damage Index Using Frequency Analysis

As explained in Chapter 3, a damage index was used to investigate whether it is possible to detect the existence and size of delamintion.

Specimen Sub-R1 was tested using a signal having 30 kHz and a two sinusoidal burst with an incident angle of 30° and a probe separation of 340 mm (Figure 22).Four different tests were repeated three times each on specimen Sub-D1 and FFT analyses were carried out (Figure 23). The specimen was tested at line L2 through L5. Each line represented a different delamination size (Figure 22). Delamination lengths were defined as the following: L1 was equal to 230 mm, L2 was equal to 160 mm, L3 was equal to 90 mm, L4 was equal to 20 mm, and L5 was equal to zero mm. The measurement was taken three times for each spacing.

Figure 23 through Figure 27 show the results of the FFT analyses. Figure 28 shows the average of each of the FFT measurements.

All of the FFT tests were then analyzed using Equation 7 where the baseline amplitude, A^0, was taken as the average of the FFT amplitudes of the tests on specimen Sub-R1. Figure 29 shows the damage index as a function of the delamination size. The figure shows that the damage index increased with increasing the delamination size.

The frequency of 100 kHz was also tested to determine if there was a change in sensitivity of the damage index with higher frequency (Figure 30). Similar to results from the 30 kHz frequency, the damage index increased with increasing delamination size.

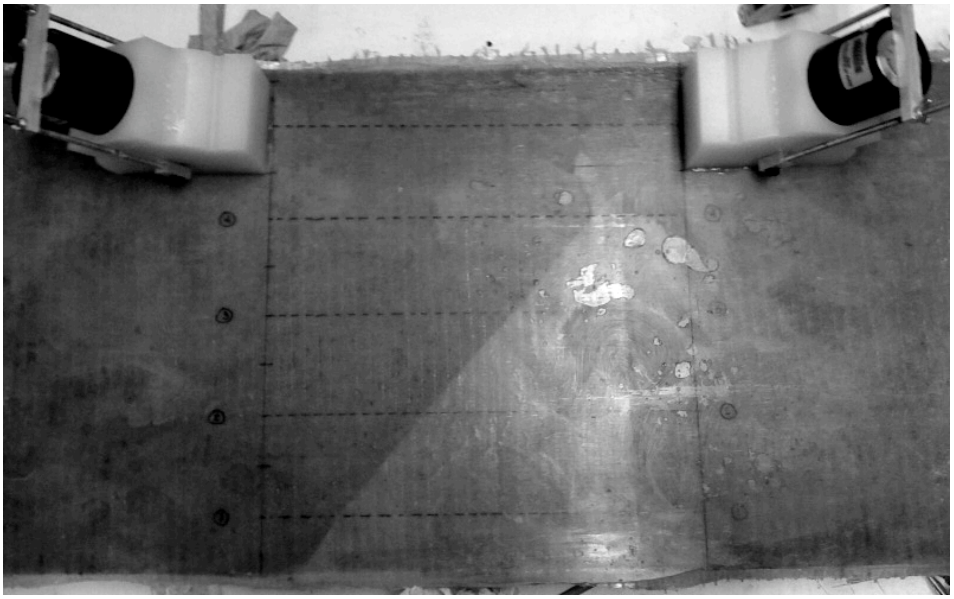

Figure 22. Test over flaw

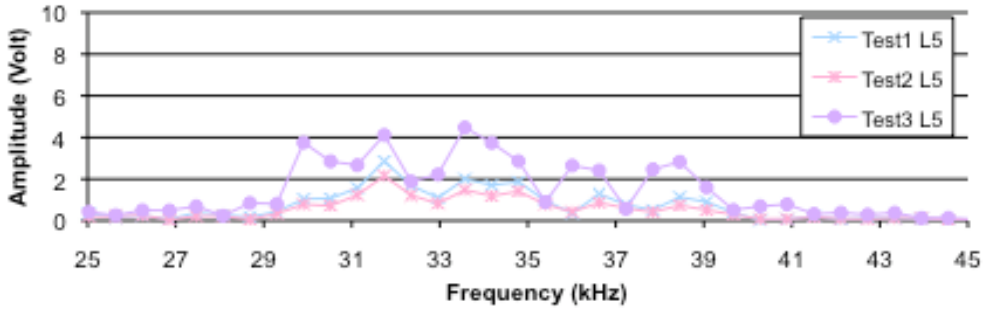

Figure 23. FFT for tests on specimen Sub-R1 (no delamination)

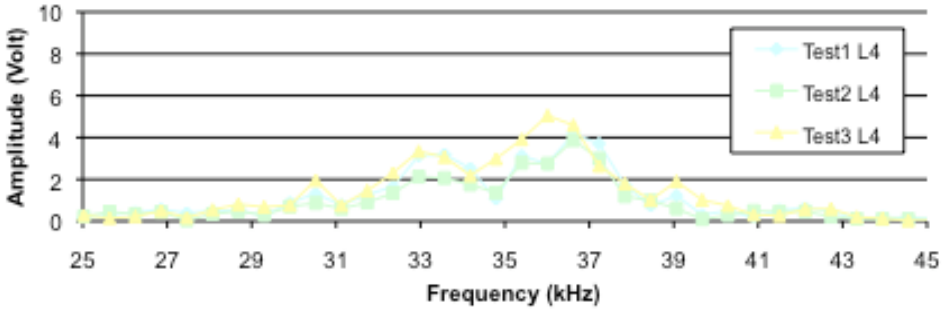

Figure 24. FFT for tests on specimen Sub-D1 having a delamination length of 20 mm

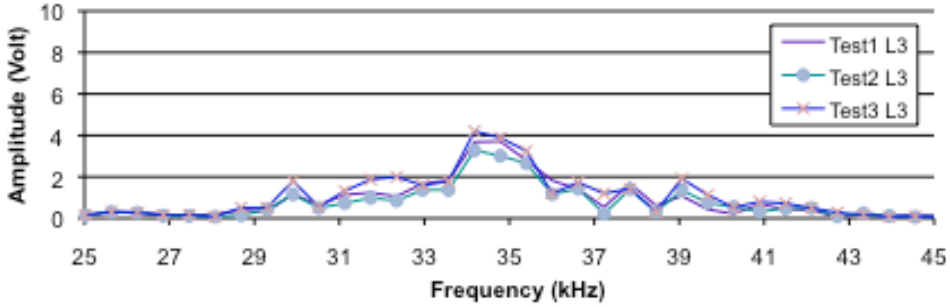

Figure 25. FFT for tests on specimen Sub-D1 having a delamination length of 90 mm

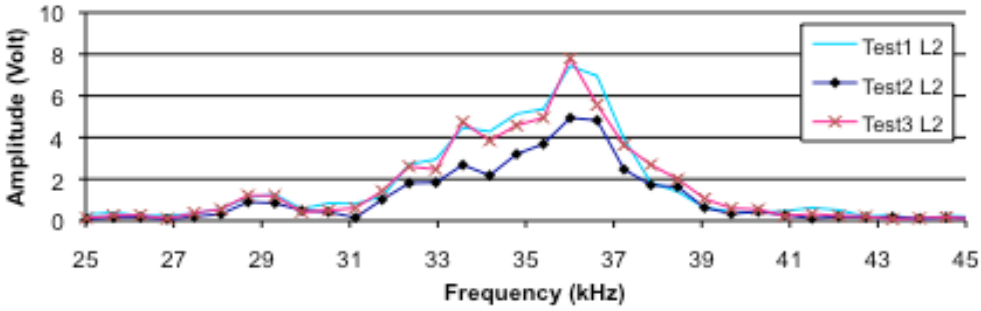

Figure 26. FFT for tests on specimen Sub-D1 having a delamination length of 160 mm

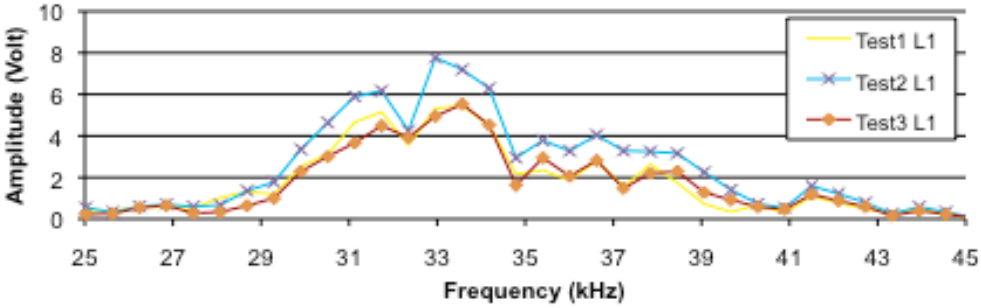

Figure 27. FFT for tests on specimen Sub-D1 having a delamination length of 230 mm

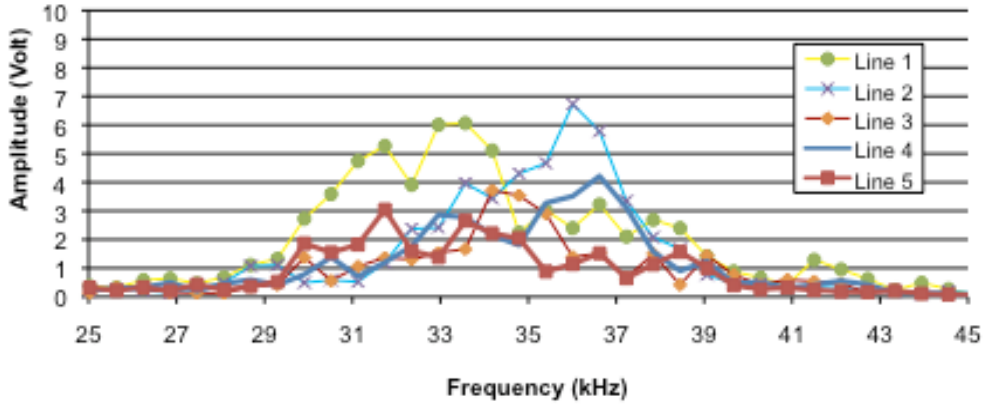

Figure 28. Average FFT for 30kHz test on Sub-D1

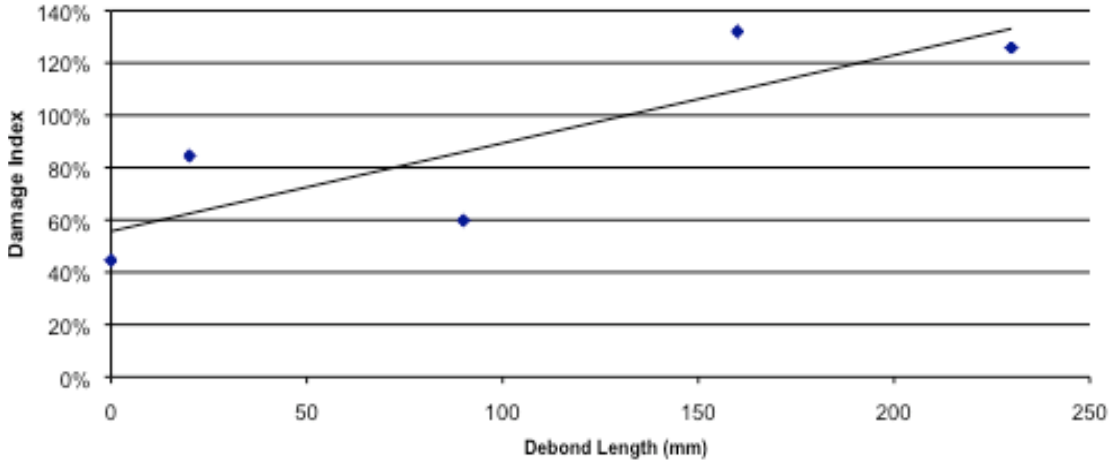

Figure 29. Damage index for Sub-R1 tested at 30 kHz and a 340 mm spacing between transducers

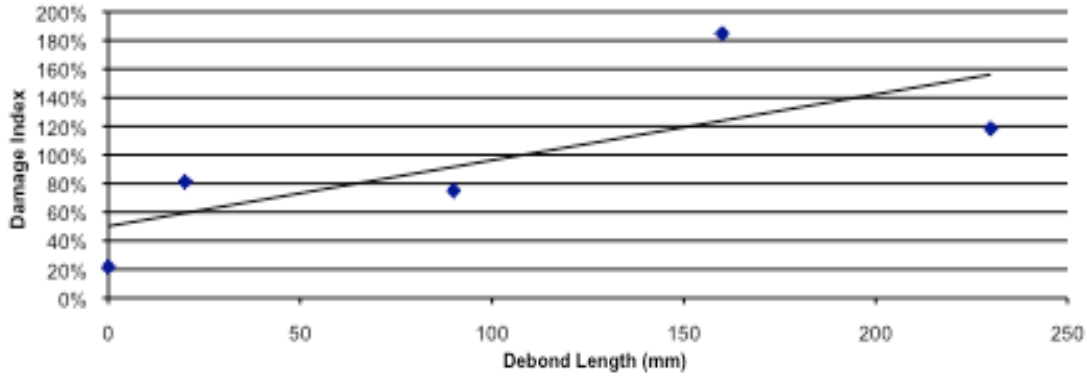

Figure 30. Damage index for Sub-R1 tested at 100 kHz and a 340 mm spacing between transducers

4.3.1 Far- Field and Near Field

This section investigates the maximum distance at which the actuator and receiver can be spaced before a flaw is no longer detectable. The test was taken at three different spacings, 340 mm, 530 mm and 720 mm, while keeping the flawed region in the center. Figure 31 shows that somewhere between 530 mm and 720 mm the damage index begin to dwindle off, only providing a maximum damage index of approximately 72%. This does not follow the increasing trend in the damage index of the other tests having smaller separation distances. However, the damage index values for all separation distances were greater than the damage index of the baseline specimen. Trend lines were fitted to the data. The R^2 values were as follows: 340 mm test had an R^2 of .693, 530 mm test had an R^2 of .832, and 720 mm test had an R^2 of .078.

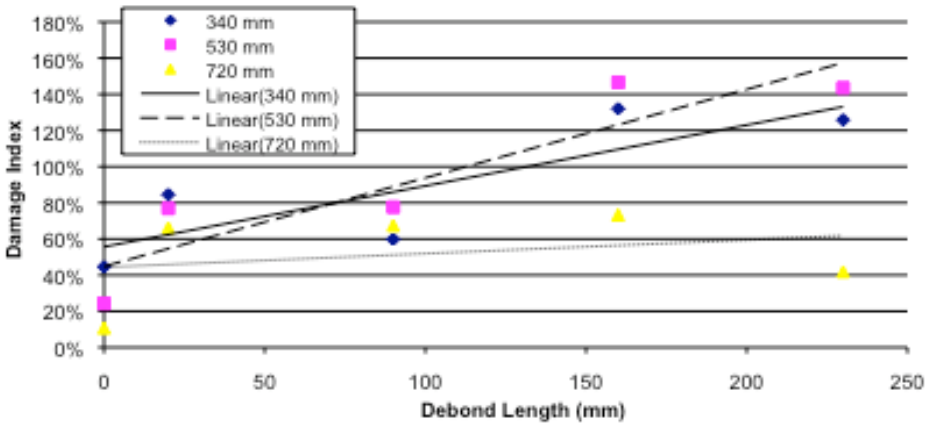

Figure 31. Damage index for Sub-R1 at 30 kHz

4.4 Effect of FRP thickness

The thickness of the fiber layer was investigated since it is common in practice to use more than one layer of FRP to meet the action demand on the retrofitted column. This sample was prepared similarly to Sub-R1, but instead contained 3 layers of FRP. The damage index for Sub-R3 appears to not have a real trend with flaw size. However, for all

delamination sizes, the damage index was higher than the damage index of the well-retrofitted specimen (Figure 32). This test was also done at an incident angle of 30 degrees and 30 kHz transmitting frequency. Trend lines were fitted to the data. The R^2 values were as follows: 340 mm test had an R^2 of .070, 530 mm test had an R^2 of .375, and 720 mm test had an R^2 of .084.

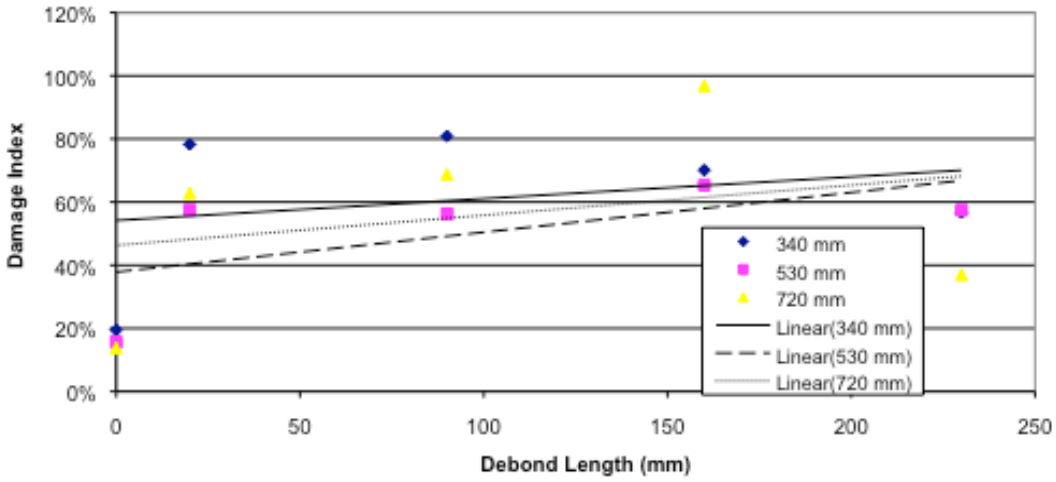

Figure 32. Damage index for Sub-R3 tested at 30 kHz

4.5 Concrete Debond

This section investigates whether the Lamb waves are able to detect debonding of the concrete cover. The test setup was the same as the previous method and the substrata crack length varied from zero to 275 mm. The debond region is the trapezoidal shape shown in Figure 33. The distances between the transmitter and receiver probes were 340 and 530 mm as was done in testing the substrate specimens. However, the 720 mm region could not be tested because the surface conditions were found to be very poor, not allowing the probe to rest flush on the surface. Figure 34 shows the damage index for the different debond lengths. As shown in the figure, the damage index for the debonded

specimen was approximately double the base line specimen. However, the damage index was approximately constant regardless of the debond size. Trend lines were fitted to the data. The R^2 values were as follows: 340 mm test had an R^2 of .364 and the 530 mm test had an R^2 of .235.

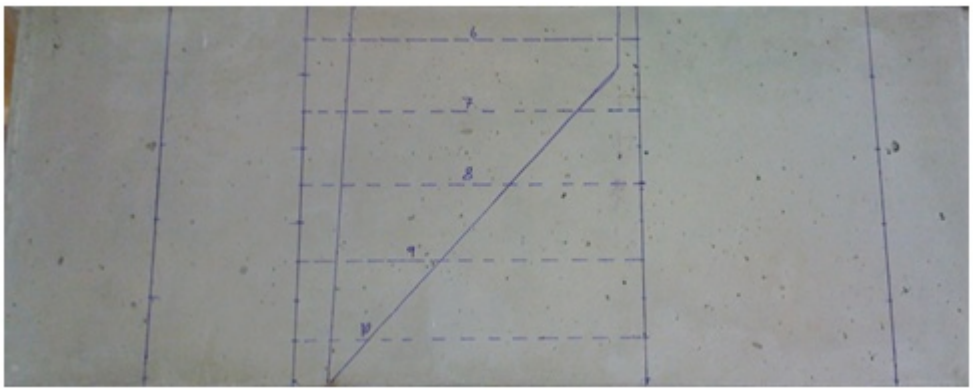

Figure 33. Substrata crack drawn on surface of concrete before applying FRP

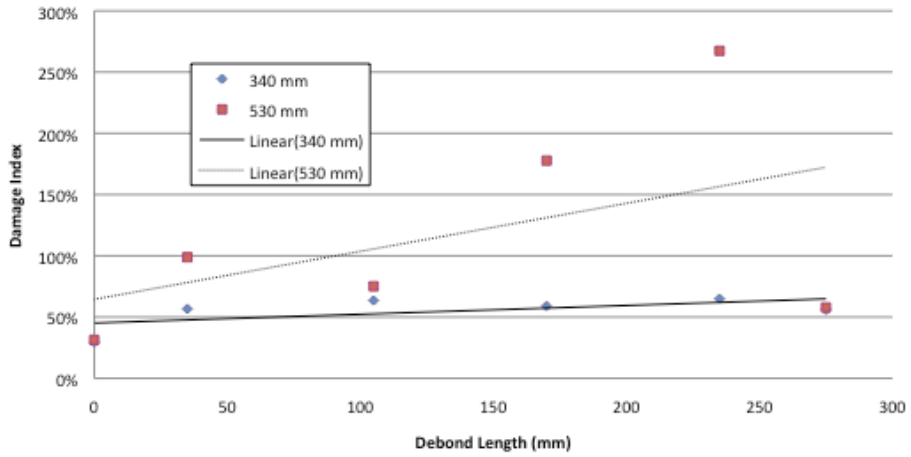

Figure 34. Damage index for specimen Col-B

4.6 Delamination (Column)

The purpose of this test is to investigate how a full depth section would affect the detection of surface delaminations. The 340 and 530 mm spacings show potential for a gradually increasing damage index as the flaw increases, but all the tests show a substantial increase compared to that of the undamaged region, as seen in Figure 35.

Trend lines were fitted to the data. The R^2 values were as follows: 340 mm test had an R^2 of .828, 530 mm test had an R^2 of .809, and 720 mm test had an R^2 of .124.

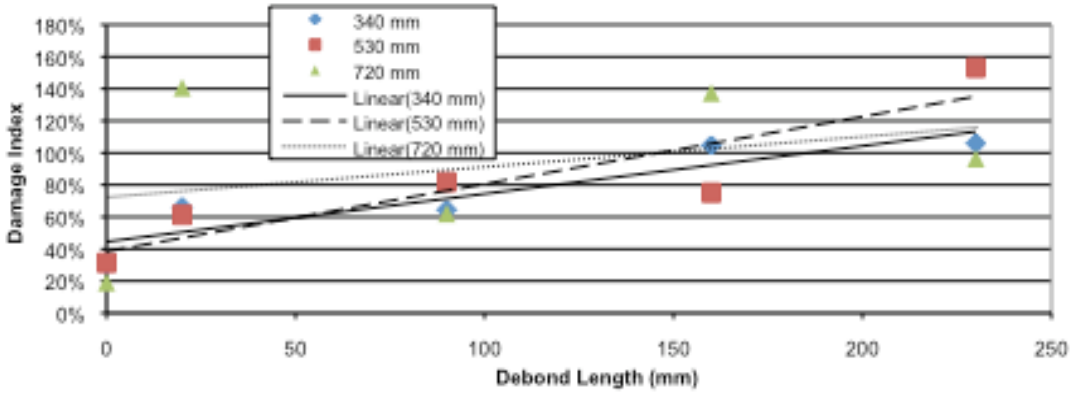

Figure 35. Damage index for Col-R1

4.7 PZT Application

In this section the effect of the type of the probe on the transmitted and received signals was investigated. The commercial probes were replaced by PZT wafers (Figure 36). The PZTs were adhered to the surface using the same epoxy as was used for adhering the fiber. The resonant frequency for the chips is 1.5 MHz but they are able to transmit and receive various frequencies through the function generator. The test on Sub-D1 was repeated using the PZT's to investigate the usefulness of these probes. The first test was transmitted at 1 MHz, which is too high for the theoretical range but was tested because it is near the resonance frequency (Figure 37). The next test was taken at 100 kHz and the third test was taken at 50 kHz at an amplitude of .5 volt (Figure 38 and Figure 39). The previous tests were taken at an amplitude of 20 volts, but this could not be repeated because the amplitude of the lower frequencies exceeded the receiver. Also, 30 kHz was not achievable using these specific PZT chips because the frequency was out of their range and a clear signal was not detectable. In addition, the 880 mm PZT

separation was found to have some sort of error in the data, possibly due to weakening of the wire leads as the final tests were being taken.

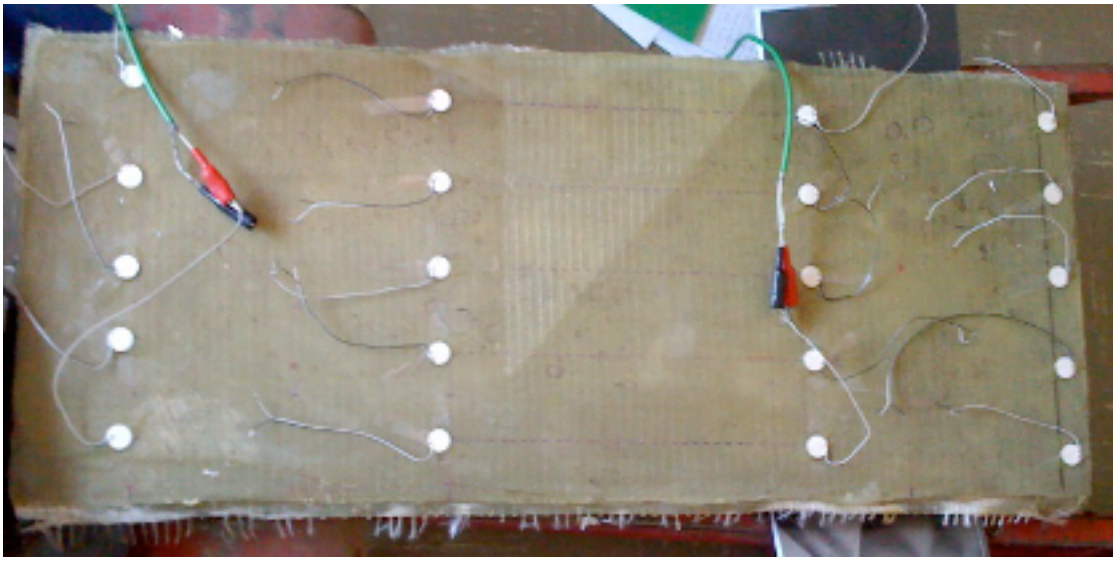

Figure 36. Sub-D1 specimen with adhered PZT wafers

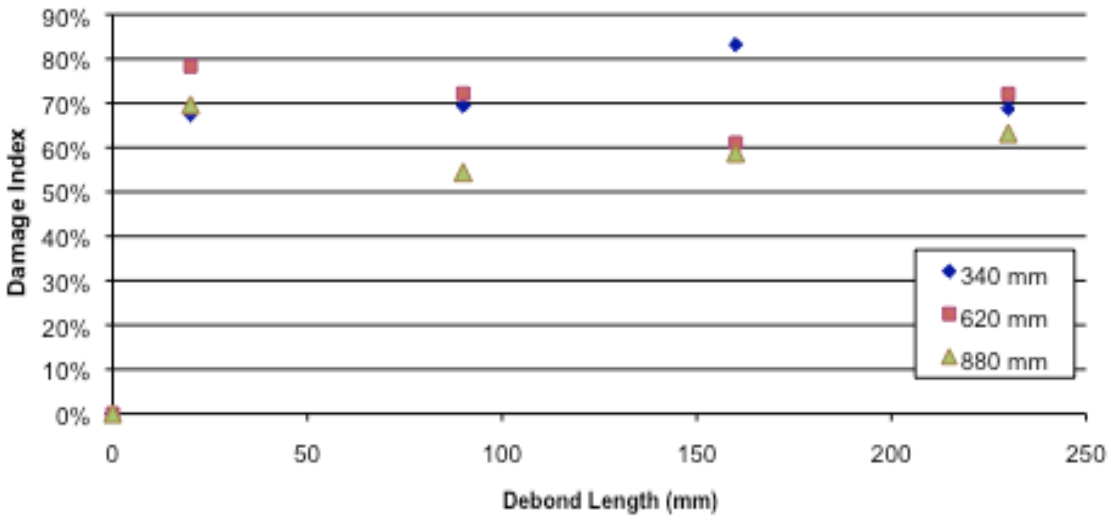

Figure 37. Damage index of Sub-R1 using PZT wafers at 1 MHz

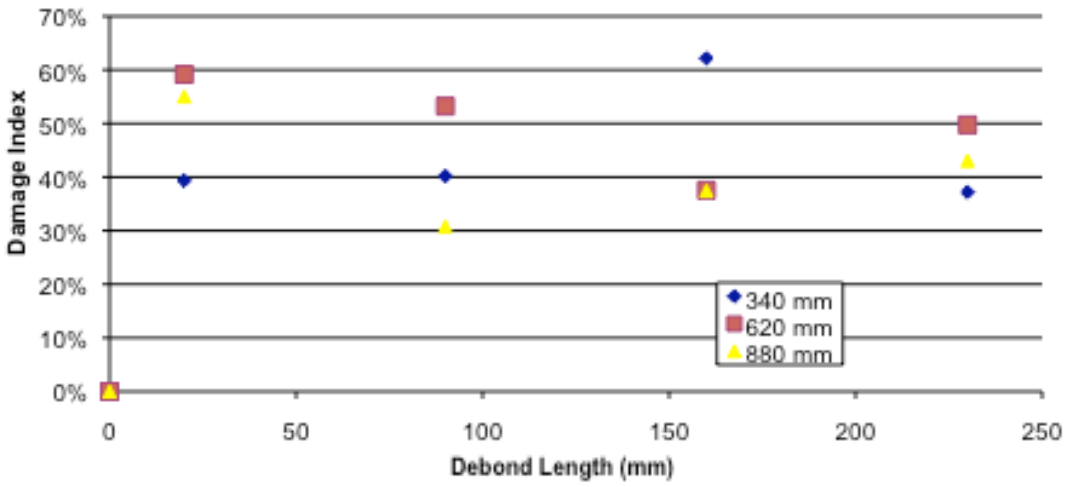

Figure 38. Damage index of Sub-R1 using PZT wafers at 100 kHz

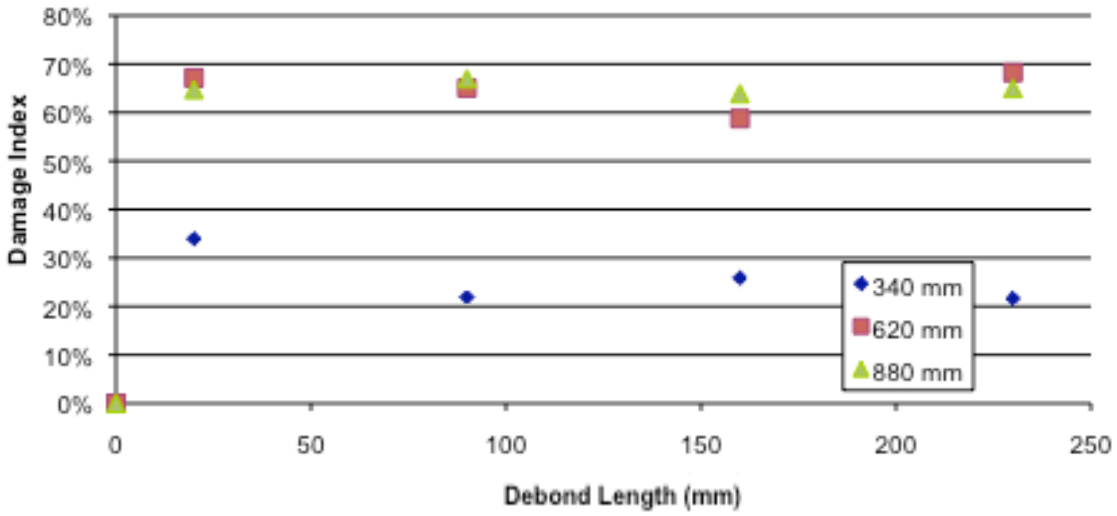

Figure 39. Damage index of Sub-R1 using PZT chips at 50 kHz

Chapter 5: Discussion and Conclusions

5.1 Results

The results for the STFT were very conclusive that it did not work. There was little or no consistent correlation. It was difficult to determine if the measured values were legitimately corresponding to a specific point on the dispersion curve or if the lines were so close that the dots appeared to show a possible solution. As for the commercial probe tests and coupling angle wedge, most of the tests appeared to show a slight trend of an increase of the damage index as the debond length increased. This trend was consistent among all of the conditions that used this method. It appeared that for the majority of the tests, the 530 mm probe spacing showed a higher R2 value. Finally, the PZT wafer method was found to be lacking in conclusive data. There was a consistent correlation that the debond was present because there was an increase in the damage index. However, there was no trend to decipher between the debond lengths.

5.2 Variation in Test results

This testing method relied strongly on the coupling between each surface. These surfaces include the probe to wedges probe mount, probe mount to curved surface of wedge, and wedge to specimen. This was necessary for the transmitting and receiving probe. If one of these regions was not properly coupled, the signal would appear weak or not appear at all. After changing the angle several times, a major concern involved the reapplication of the coolant to the curved surface and the probe mount because some would be scraped out with each alteration.

Also, surface conditions of the FRP overlay was of concern. In an attempt to make the FRP surface smooth so coupling could be possible, a piece of countertop laminate was waxed and firmly lowered onto to the specimen, compressing the wet epoxy coated fiber before it had cured to the concrete. This was effective to create a flat surface, however there were regions where air pockets forms. This required an excess of couplant gel to fill the voids in the surface and properly couple the surfaces. Because of this, the couplant material was in the testing region and misrepresenting the signal in the fiber and concrete.

5.3 Conclusion

This research showed that there is potential to detect delaminations. The test results showed that the existence of the delamination did not result in any systematic shift in the frequency of the test specimens using the Lamb wave dispersion curve. However, using the damage index showed potential to detect the existence of a delamination or debonding. In the case of delamination, the damage index is sensitive to the delamination size. The damage index increased with increasing the delamination size.

Overall, the commercial probes were the most effective, but the actual propagation of lamb waves is very questionable. The incident angle of 30 degrees is in the realm of the longitudinal incident angle. Some other form of a guided wave was more than likely generated in this test. The 530 mm probe spacing appeared to consistently give a higher R2 value, possibly indicating that given the testing procedures above, 530 mm is near the ideal probe spacing to detect the various flaw conditions.

However, the less expensive PZT wafers were found to be unsuccessful. This was due to the fact that there was little to no variability in the control tests on the fully bonded region because the wafers were not movable and permanently coupled. When the control was compared to itself, it appeared that the baseline had no imperfections. This was due to lack in variation from coupling which, was seen in the commercial probes. There should have been at least two PZT wafers attached in the control region of the sample to provide variation, which would be expected based on the different aggregate conditions within the concrete

Appendix A

A 1. Derivation of Wave Velocity Equations

$$c_1 = \sqrt{\frac{\lambda + 2\mu}{\rho}}, \lambda = \frac{E\nu}{(1+\nu)(1-2\nu)}, \mu = \frac{E}{2(1+\nu)}$$

$$c_1 = \sqrt{\frac{\frac{E\nu}{(1+\nu)(1-2\nu)} + \frac{E}{(1+\nu)}}{\rho}}$$

$$c_1 = \sqrt{\frac{E\nu + E(1-2\nu)}{(1+\nu)(1-2\nu)\rho}}$$

$$c_1 = \sqrt{\frac{E(\nu + (1-2\nu))}{(1+\nu)(1-2\nu)\rho}}$$

$$c_1 = \sqrt{\frac{E(1-\nu)}{(1+\nu)(1-2\nu)\rho}}$$

$$c_2 = \sqrt{\frac{\mu}{\rho}}, \mu = \frac{E}{2(1+\nu)}$$

$$c_2 = \sqrt{\frac{E}{2\rho(1+\nu)}}$$

A 2. Dispersion Curve Program

```
clear
```

```
clc
%%%%%%%%%%%%%%   INPUT %%%%%%%%%%%%%%%%%%%%

E_=31956077323; %value back calculated for assuming nu CONCRETE
nu=.2; %poisson raio
roe=2243; %deinsiyt in kg/m^3

cL=(E_*(1-nu)/(roe*(1+nu)*(1-2*nu)))^.5
cS=(E_/(2*roe*(1+nu)))^.5

%%%%%%%%%%%%%%%%%%%%%%%%%%%%%%%%%%%%%%%%%%%%%%%
% cL=6320; Aluminum
% cS=3130;

n=14000;
max=30000;      %maximum number of outputted results
Result=zeros(6,max);
VEL=zeros(2,max);
FD=zeros(2,max);
Jval=zeros(2,max);
k=2; %%%%% increment of phase velocity "c"%%%%

Q=1;
for anti=1:2        %%%changes symmetric to antisymmetric
  if anti==1
      exp=1;
      count=1;
  else
      exp=(-1);
      count=1;
      disp('half way')
  end
  for gap=1:n
      c=0;
      w=gap*25;      %%%%d*w increment

      while c<10000

        if c<cS
        j_2=tanh(w*((((c^2-cS^2)/(cS^2*c^2))^.5)/i))/(tanh(w*(((c^2-
cL^2)/(cL^2*c^2))^.5)/i))-(4*((((c/cL)^2-1)*((c/cS)^2-1))^.5/(2-
(c/cS)^2)^2))^(exp);
        elseif c<cL
        j_2=tan(w*(((c^2-cS^2)/(cS^2*c^2))^.5))/(tanh(w*(((c^2-
cL^2)/(cL^2*c^2))^.5)/(i)))-exp*(4*(((((c/cL)^2-1)*((c/cS)^2-
1))^.5)/i/(2-(c/cS)^2)^2))^(exp);
        else
        j_2=tan(w*(((c^2-cS^2)/(cS^2*c^2))^.5))/(tan(w*((c^2-
cL^2)/(cL^2*c^2))^.5))+(4*((((c/cL)^2-1)*((c/cS)^2-1))^.5/(2-
(c/cS)^2)^2))^(exp);
        end

              if c==0
                  j_1=j_2;
              else
              end
```

```
          if ((j_2*j_1)<0)&&(abs((j_2-j_1))<10)
                [c,j_2]=Iterate(c,k,w,cS,cL,exp); %calls a fucntion to
iterate to get value closer to zero

                 VEL(anti,count)=c;
                 FD(anti,count)=w/pi;
                 Jval(anti,count)=j_2;

                    if abs(j_2)>1
                    else
                    count=count+1;

                    end
               j_1=j_2;
               c=c+k;
          else
               j_1=j_2;
               c=c+k;
          end
            if count>max
             break
            else
            end
      end
  end
end
%%%%%%%%%%%%%%%%%FILLER%%%%%%%%%%%%%%%%%%%%%%
for n=1:2
    for q=1:max
Result(3*n-2,q)=VEL(n,q); %%%Jval- THis is the value of how close to
zero the program made it.
Result(3*n-1,q)=FD(n,q);  %%%%Frequency (F*D)
Result(3*n,q)=Jval(n,q); %%%%%%%%phase velocity
    end
end
xlswrite('Plotvalues.xls', Result')
```

A 3. Iteration Function

```
function [c,j_2]=Iterate(c,k,w,cS,cL,exp)

    ko=.01;
co=c+k*2;
c=c-k;
for it=2:2
    c=c-ko^(it-1);

        if c<cS
        j_2=tanh(w*((((c^2-cS^2)/(cS^2*c^2))^.5)/i))/(tanh(w*(((c^2-
cL^2)/(cL^2*c^2))^.5)/i))-(4*((((c/cL)^2-1)*((c/cS)^2-1))^.5/(2-
(c/cS)^2)^2))^(exp);
        elseif c<cL
```

```
        j_2=tan(w*(((c^2-cS^2)/(cS^2*c^2))^.5))/(tanh(w*(((c^2-
cL^2)/(cL^2*c^2))^.5)/(i)))-exp*(4*(((((c/cL)^2-1)*((c/cS)^2-
1))^.5)/i/(2-(c/cS)^2)^2))^(exp);
        else
        j_2=tan(w*(((c^2-cS^2)/(cS^2*c^2))^.5))/(tan(w*((c^2-
cL^2)/(cL^2*c^2))^.5))+(4*((((c/cL)^2-1)*((c/cS)^2-1))^.5/(2-
(c/cS)^2)^2))^(exp);
        end
    j_1=j_2;

    while ((j_2*j_1))>0

        c=c+ko^it;

        if c>co
          break
        else
            j_1=j_2;
        end
        if c<cS
        j_2=tanh(w*((((c^2-cS^2)/(cS^2*c^2))^.5)/i))/(tanh(w*(((c^2-
cL^2)/(cL^2*c^2))^.5)/i))-(4*((((c/cL)^2-1)*((c/cS)^2-1))^.5/(2-
(c/cS)^2)^2))^(exp);
        elseif c<cL
        j_2=tan(w*(((c^2-cS^2)/(cS^2*c^2))^.5))/(tanh(w*(((c^2-
cL^2)/(cL^2*c^2))^.5)/(i)))-exp*(4*(((((c/cL)^2-1)*((c/cS)^2-
1))^.5)/i/(2-(c/cS)^2)^2))^(exp);
        else
        j_2=tan(w*(((c^2-cS^2)/(cS^2*c^2))^.5))/(tan(w*((c^2-
cL^2)/(cL^2*c^2))^.5))+(4*((((c/cL)^2-1)*((c/cS)^2-1))^.5/(2-
(c/cS)^2)^2))^(exp);
        end
    end
end
end
```

A 4. STFT Program

```
clc
clear
angle=50;               %in degree
D=17;                   %distance between probes ****Specific to the
big plastic wedges****
ceiling=10000;          %upper limit on accepting phase velocity
cutoff=1500;            %phasve veloctiy cutoff. If lower than
possible-not saved
w=200;                  %even numbers when divisable by 2 only --------
Lenght of hanning window
ol=.25;                 %must be divisable value of "w" ----amount of
overlap in percent
Thick=53;               %thickness in millimeters
GM = xlsread ('40khz 50 deg 17cm 5833488.xls');
GM = GM';
GM = GM (:);
Fs=5833488;             % Sampling rate
t=0:1/Fs:1;
```

```
v2=1;
v=1;                    %used as a counter
ol=1/(1-ol);            %Converts "ol" into a value that can be used by
the loops below
T= 1/Fs;                              % Sample time
L=length(GM);                         % data length
t=(0:L-1)*T;                            %No changes
angle=angle*pi/180;

D=D+(6.35-2.5*tan(angle)+6.3/2);
lw=(7+2.5/cos(angle)); %lenght that sound is in wedge

 tminus=lw/2073.04/100; %time offset due to signal in wedge

for h=1:w
    W(h)=.5*(1-cos(2*pi*h/w));            %creating hanning window
end


for j=1:round(L/w*ol-3)
%Ct=t((j)*w/ol)-t(w/ol);            %time beginning of window
Ct=t(((j-1)*w/ol)+w/2);             %time at center of window
    for q=1:L
        GM_(q)=(0);                       %clears the "window" of data
    end

    for k=1:w
        GM_((j-1)*w/ol+k)=GM((j-1)*w/ol+k)*W(k);   %assigns value from
original vector and then applies hanning window
    end

if Ct-tminus>0
if D/(Ct-tminus)/100>cutoff
    if D/(Ct-tminus)/100<ceiling
NFFT=2^nextpow2(L);                    %Next highest power of 2 greater
than or equal to L to calculate fft_________No changes
Y=fft(GM_,NFFT);                       %Pay attention of the
gravitional acceleration
NumUniquePts = ceil((NFFT+1)/2);
Y=Y(1:NumUniquePts);
Y=Y/(L);
Y=(abs(Y)).^2;
Y(2:end -1) = Y(2:end -1)*2;
f=(0:NumUniquePts-1)*Fs/NFFT;         %plot(f,Y)         %No changes
GG=length(Y);
    for z=1:GG
       Amp(j,z)=Y(z);
        time(j,z)=(Ct-tminus);
        freq(j,z)=f(z);

        Vel(j,z)=D/(Ct-tminus)/100;          %Velocity in meters per
second

    end


   for h=1:GG
```

```
       Q(h+1)=Y(h);           %shift up the values so zero can be
inserted
   end

    for h=2:GG+1
        Q(1)=0;Q(GG+2)=0;
        if Q(h)-Q(h+1)>0            %%Selects maximum values

                if Q(h)-Q(h-1)>0
                if f(h)*Thick/1000>150


                Max(v)=f(h)*Thick/1000;   %output frequency in kHz
                vel(v)=D/(Ct-tminus)/100;
                v=v+1;
                end
                end

        end
    end
 end
end
end
end

for k=1:(v-1)
    Result(k,1)=Max(k);
    Result(k,2)=vel(k);
end
xlswrite('Plotvalues.xls',Result) %output to excel file
```

Appendix B

B 1. Retrofitted Angle and Frequency Tests

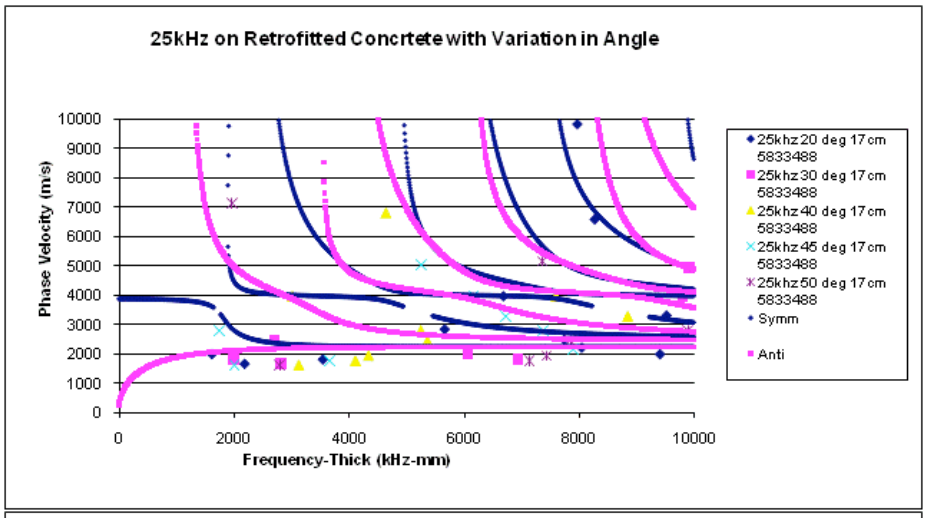

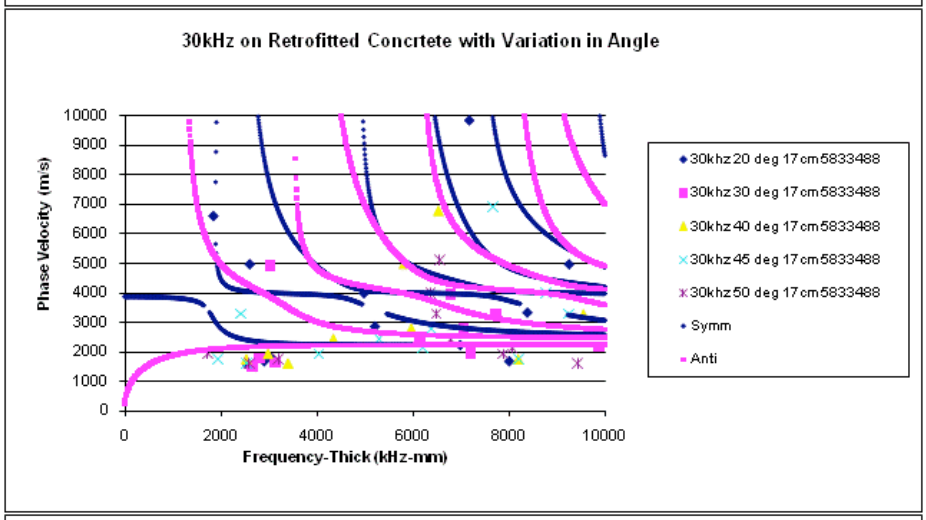

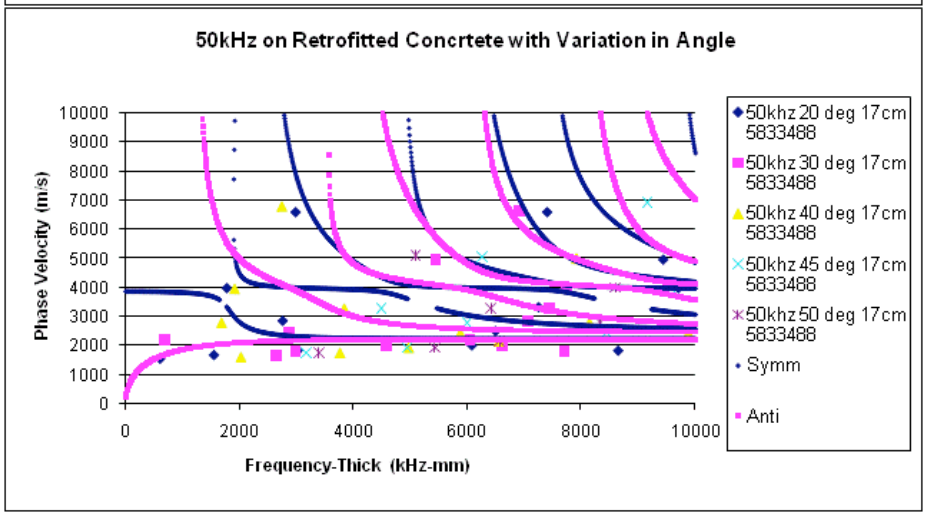

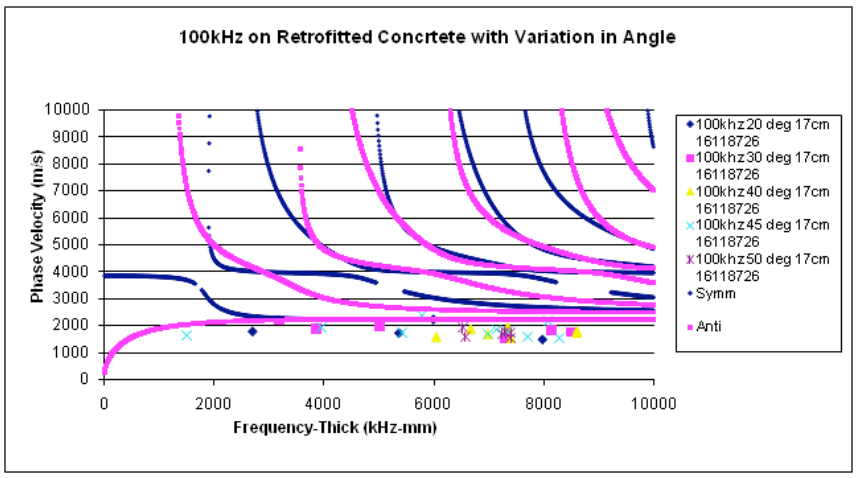

B 2. Delaminated Test

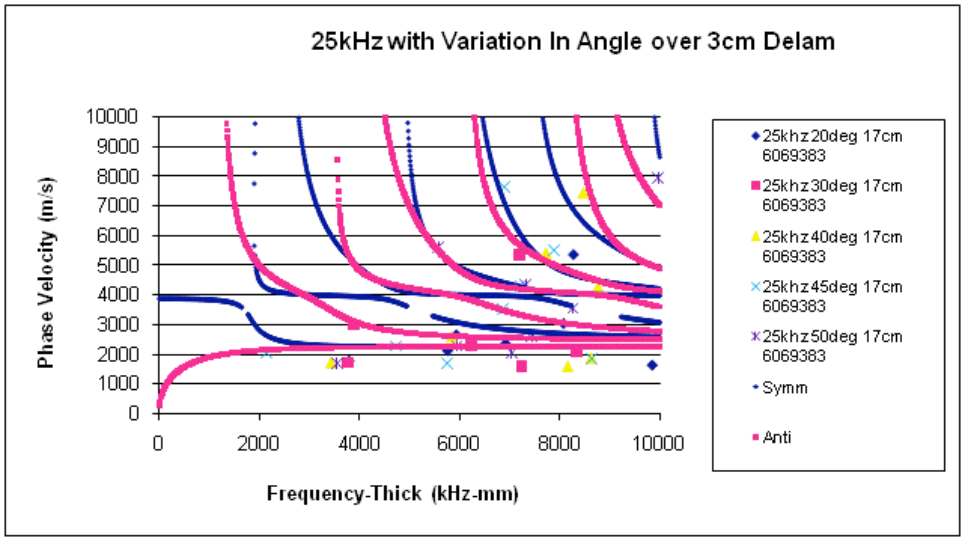

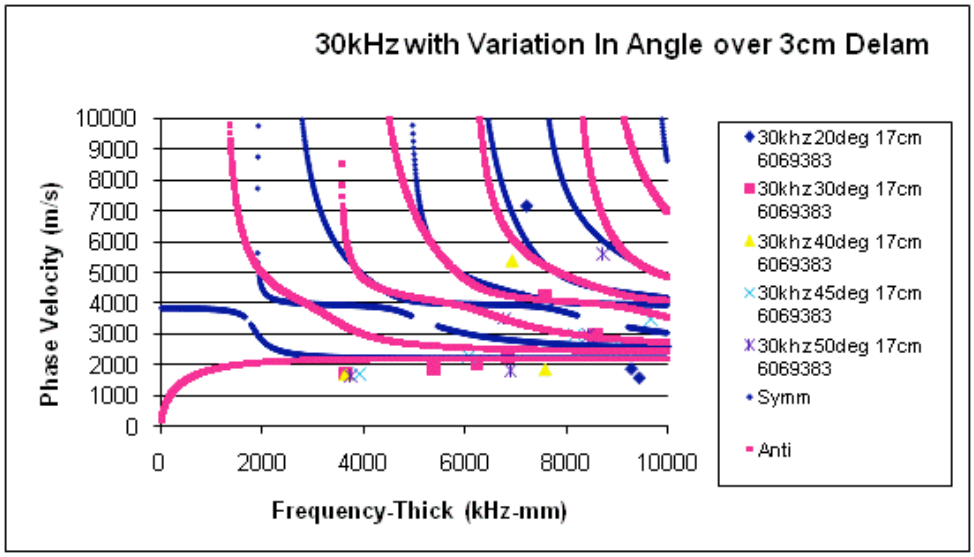
30kHz with Variation In Angle over 3cm Delam
Phase Velocity (m/s)
10000
9000
8000
7000
6000
5000
4000
3000
2000
1000
0
0
2000
4000
6000
8000
10000
Frequency-Thick (kHz-mm)
30khz 20deg 17cm 6069383
30khz 30deg 17cm 6069383
30khz 40deg 17cm 6069383
30khz 45deg 17cm 6069383
30khz 50deg 17cm 6069383
Symm
Anti

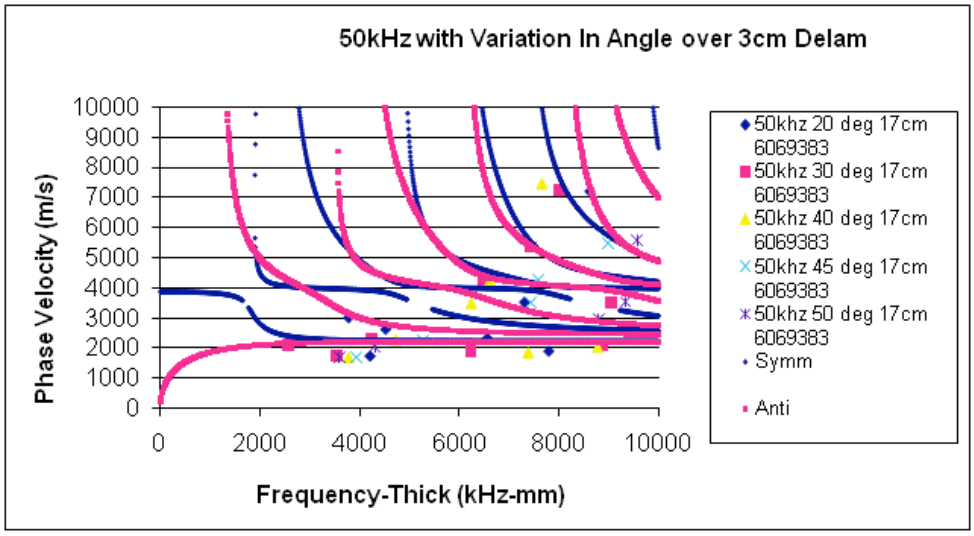
50kHz with Variation In Angle over 3cm Delam
Phase Velocity (m/s)
10000
9000
8000
7000
6000
5000
4000
3000
2000
1000
0
0
2000
4000
6000
8000
10000
Frequency-Thick (kHz-mm)
50khz 20 deg 17cm 6069383
50khz 30 deg 17cm 6069383
50khz 40 deg 17cm 6069383
50khz 45 deg 17cm 6069383
50khz 50 deg 17cm 6069383
Symm
Anti

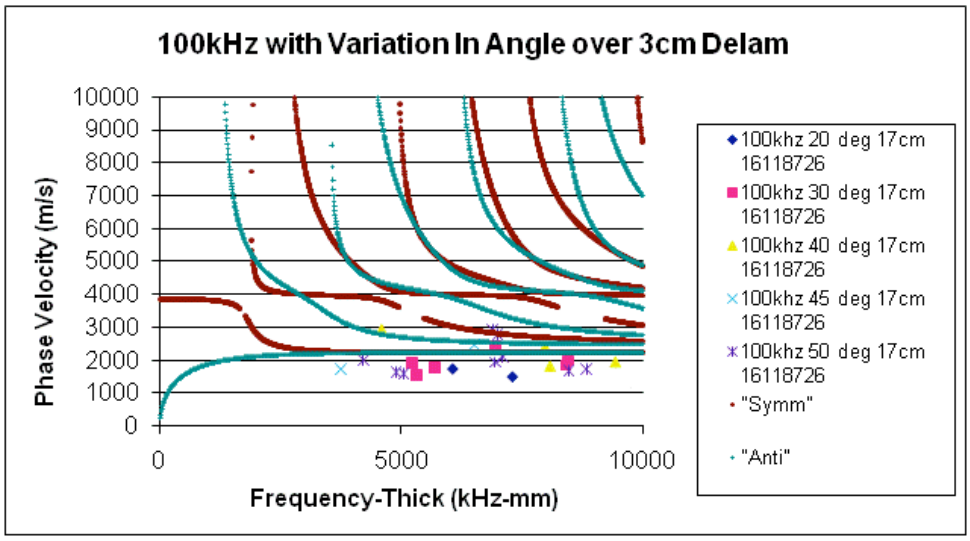
100kHz with Variation In Angle over 3cm Delam
Phase Velocity (m/s)
10000
9000
8000
7000
6000
5000
4000
3000
2000
1000
0
0
5000
10000
Frequency-Thick (kHz-mm)
100khz 20 deg 17cm 16118726
100khz 30 deg 17cm 16118726
100khz 40 deg 17cm 16118726
100khz 45 deg 17cm 16118726
100khz 50 deg 17cm 16118726
"Symm"
"Anti"

References

Bray, Don E., and R.K. Stanley. 1997. Nondestructive Evaluation: A Tool in Design, Manufacturing, and Service. CRC Press, New York, NY.

Giurgiutiu V., Harries K., Petrou M., Bost J., and Quattlebaum J. (2003). “Disbond detection with PWAS in RC structures strengthened with FRP composite overlays” Earth. Eng. Eng. Vib., 2(2).

Hong S., and Harichandran R. (2005). “Sensors to Monitor CFRP/concrete bond in beams using electrochemical impedance spectroscopy” J. Comp. Cons., 9(6).

Huang, W. 1999. Verbal communication. Digital Wave Corporation. Englewood, CO.

Jung Y. C., Kundu T., Ehsani M., (2001). “Internal discontinuity detection in concrete by Lamb waves” Mat. Eval., 59 (3).

Kundu T., Ehsani M., Masolv K. I., Guo D., (1999). “C-scan and L-scan generated images of the concrete/GFRP composite interface” NDT&E Int., 32 (2).

Luangvilai K., Punurai W., and Jacobs L. (2002). “Guided Lamb wave propagation in composite plate/concrete component”, Eng. Mech., ASCE, Vol. 128(12).

NCHRP (2006). “Field inspection of in-service FRP bridge decks” Rep. 564, Wash. D.C.

Rose, Joseph L. (1999). Ultrasonic Waves in Solid Media. Cambrige University Press.

Tucker, Brian J. (2001). Ultrasonic Plate Waves in Wood-Based Composite Panels. Washington State University.